

Donepezil and Embelin loaded Nanostructured lipid carriers for direct brain delivery as an intervention for Alzheimer's disease: Formulation design, Optimization and Evaluation

Mohd Humair Ali

Jamia Hamdard

Ozair Alam

Jamia Hamdard

Asad Ali

Jamia Hamdard

Mohd Uzair Ali

Jamia Hamdard

Suhel Parvez

Jamia Hamdard

Eman Aldosari

King Saud University

Sanjula Baboota

Jamia Hamdard

Javed Ali (✉ javedaali@yahoo.com)


Jamia Hamdard

Research Article

Keywords: Alzheimer's disease, Donepezil hydrochloride, Embelin, Nanostructured lipid carriers, Intranasal, in vitro

Posted Date: August 31st, 2023

DOI: <https://doi.org/10.21203/rs.3.rs-3276213/v1>

License:  This work is licensed under a Creative Commons Attribution 4.0 International License. [Read Full License](#)

Abstract

Donepezil hydrochloride (DPL) and Embelin (EMB) loaded Nanostructured Lipid Carriers (NLCs) have been developed and optimized to achieve optimal drug loading, safer nasal delivery, effective neuronal/cell uptake, enhanced brain accessibility, controlled release, and desired therapeutic effect. Molecular docking studies demonstrated that both drugs bind effectively to AchE with interaction energies of -48.5319 and -65.7525, respectively, indicating a synergistic approach. The hydrophobic interactions with target proteins facilitate the transportation of drugs through brain hydrophobic channels to provide a desired pharmacological response. N2a cell line investigation advised a 1:1 ratio of DPL and EMB to have the greatest possible synergistic effect based on the MTT assay. NLCs were fabricated by hot emulsification probe sonication method and optimized using QbD-based Central Composite Rotatable Design (CCRD). Optimized NLCs with a diameter of 180.2 nm were suitable for axonal uptake. A low PDI score of 0.37 and ZP of -12 mV indicated a uniform monodisperse system with persistent and stable dispersion properties. The NLCs demonstrated sustained drug release, DPL released at 90.72 ± 1.00 percent and EMB at 81.30 ± 0.52 percent in 24 hours. The Korsmeyer-Peppas model proved to be the most accurate fit due to its strong correlation. Ex vivo permeation and CLSM studies revealed superior goat nasal mucosa penetration of NLCs over suspension with a higher fluorescence level, up to 35 μm . NLCs treated nasal mucosa exhibited no erosion or interstitial gaps in the histopathological study. Moreover, NLCs were nontoxic and non-irritating, with a HET CAM score of 0.68 ± 0.05 , indicating safe nasal delivery. The cellular uptake study showed a preponderance of the NLCs in the Cell's cytoplasm, indicating ready uptake by N2a cells. Hence, intranasal therapy with the DPL and EMB-loaded NLCs could be a practical and promising implementation. Further *in vivo*, and clinical studies will be required to establish the formulation's efficacy in treating Alzheimer's disease (AD).

1. Introduction

Alzheimer's disease (AD) is a progressive neurodegenerative disorder characterized by the formation of extracellular amyloid plaques, intracellular neurofibrillary tangles (NFTs) as a result of tau hyperphosphorylation [1], loss of cholinergic neurons in the basal forebrain [2], mutations in the presenilin 1 (PSEN1), presenilin 2 (PSEN2), and amyloid precursor protein (APP) genes [3] microglial activation alongside inflammation, oxidative damage, iron dysregulation, and cholesterol metabolism [4]. A study conducted by Pivovara et al. inferred insulin resistance and reduced insulin signaling in the brain as one of the critical factors in AD pathology, owing to the inhibition of IDE-dependent beta-amyloid protein breakdown [5]. According to estimates, 40 million individuals worldwide have dementia, and it is likely to double every 20 years until about 2050 [6].

Donepezil hydrochloride (DPL), galantamine, and rivastigmine are acetylcholinesterase inhibitors (AChEIs) approved for AD treatment [7]. Besides, Memantine is an FDA-approved noncompetitive N-methyl d-aspartate (NMDA) receptor antagonist, which reduces NMDA-mediated ion flow and pathologically elevated glutamate levels and alleviates neuronal dysfunction [8]. DPL and memantine combinatorial therapy were also approved in 2014. Emerging disease-modifying therapies (DMTs) that interfere in the underlying pathophysiological mechanisms of the disease process that lead to cell death captivates a new area of drug research and development in AD which includes BACE inhibitors, γ secretase inhibitors, α secretase modulators, $\text{A}\beta$ aggregation inhibitors, Kinase inhibitors, Tau aggregation inhibitors, Microtubule stabilizers, immunotherapy, etc. [2, 9]. Cognitive impairment is reduced temporarily by existing treatments. The failure to traverse the blood-brain barrier, systemic side effects that restrict dosage, and complex dosing schedules are typical obstacles associated with current medications that ultimately reduce patient adherence and result in the discontinuation of therapy.

Oral administration for brain disorders is ineffective, requires a high dose, and has systemic side effects. Intranasal (IN) delivery is a promising alternative as it avoids first-pass metabolism, bypasses the blood-brain barrier (BBB) and blood-cerebrospinal fluid (CSF) barrier, and is extensively vascularized, allowing for higher drug uptake in the brain [10]. It utilizes the olfactory neuron and trigeminal pathway for drug transport directly to the brain [11] (Fig. 1), reducing the frequency and dosage. The nasal route is achieving more focus as an alternative to the parenteral route by needless avoidance; it represents the most direct method of non-invasive entry into the brain.

Drug delivery approaches to target the brain have been researched to maximize drug effectiveness, minimize degradation and loss, and reduce peripheral and systemic side effects. Approaches include chemical modifications such as prodrug, P-glycoprotein inhibition, physiological such as receptor-mediated transcytosis, and biological methods such as conjugation of drugs with antibodies, use of genomics and non-invasive techniques for direct delivery of drugs to the brain [12]. Researchers have prioritized the emergence of Nano drug delivery techniques lately, with a particular focus on lipid-based systems like Nano emulsions, SLNs, and NLCs to surmount the obstacle of BBB, attain brain targeting, ameliorate the systemic adverse effects and achieve sustainable treatment with desired therapeutic effect. These systems can efficiently deliver hydrophobic molecules and protect them from being eliminated in the nasal cavity. Scientists are also exploring the use of biomolecules, thermosensitive polymers, and mucoadhesive polymers to enhance the therapeutic potential of these lipid-based Nano systems [13].

The present research centers on developing nanostructured lipid carriers (NLCs) for drug delivery to the brain for addressing AD. The higher drug loading and entrapment of NLCs are attributed to the presence of nano-oil sections in the solid lipid matrix and the uneven distribution of liquid lipids in the solid lipid's crystal defects [14]. Including liquid lipids also maintains sub-saturation conditions of solid lipids, preventing crystallinity and polymorphic changes and providing long-term stability to the formulation. Improved brain accessibility, controlled drug release, efficient penetration into tiny capillaries and cellular uptake owing to their small size and lipophilic nature, site-specific targetability, avoidance of first-pass metabolism, and defense against P-gp efflux transporters are other significant attributes of NLCs [15]. Many strategies, such as the development of Duloxetine-loaded NLCs for depression [16], Carbamazepine loaded NLCs for Epilepsy [15], Nimodipine loaded Lactoferrin customized NLCs for ischemic stroke [17], artemether-loaded-NLCs-for-cerebral malaria [18], Curcumin loaded NLCs for brain tumor [19], Asenapine loaded NLCs for schizophrenia [20], Salvianolic acid and Bacicap loaded NLCs modified with transferrin receptor monoclonal antibody (OX26) for cerebral reperfusion injury [21] and Glial cell line-derived neurotrophic factor loaded NLCs modified with Trans activator of transcription (TAT) peptide for Parkinson [22] have been brought out which have corroborated the advantages of brain delivery of NLCs over conventional dosage forms.

DPL was chosen as a drug candidate for the current study due to its high efficacy towards AD and superior anti-Alzheimer activity than other AChE inhibitors. However, it has certain limitations, such as extensive plasma protein binding (96%) owing to long elimination half-life (70hrs), which in turn causes dose-related toxicity (gastrointestinal hemorrhage, bronchoconstriction, vagotonic effects, bradycardia, and hypotension.) [23], limited brain accessibility, first-pass metabolism, and serving as a substrate for P-gp at clinically relevant doses [24]. Based on the above findings, i.e., the challenges faced by existing formulations [tablets (oral), solutions (IV)], the molecule's superior clinical profile, and high lipophilicity, it is a suitable candidate to be formulated into a nanostructured lipid carrier (NLC). Thus, the study aims to be performed, which widens the scope of research on DPL as an intranasal NLC formulation in AD. Embelin (EMB), a naturally occurring substance found in *Embelia ribes* Burm fruits, has been reported to have a significant role in suppressing symptoms of AD in preclinical investigations by inhibiting AChE, BChE, BACE-1 as per the *in silico* studies and enzyme inhibition assays [25, 26] and elevating the expression of scavenger enzymes (SOD1 and CAT), reducing oxidative stress and lipid peroxidation, promoting neurogenesis, and contributing to synaptic plasticity (BDNF-CREB levels) [26]. Recent research has also demonstrated that EMB can ameliorate scopolamine-induced amnesia and reverse STZ-induced memory impairment in rats [26, 27]. EMB has also been reported to increase P-gp activity in LS-180 cells, an efflux pump that removes amyloid- from the AD brain [28]. These studies furnished excellent results stipulating EMB as a potent molecule for AD. Moreover, its physicochemical properties make it a good candidate for formulation into an NLC. It has been contemplated that the combination therapy of DPL and EMB could be highly effective, possess lesser side effects, and provide a synergistic effect by a multitargeted mechanistic approach.

The current work aims to prepare DPL-EMB NLCs with an emphasis on achieving optimum drug loading, safer nasal administration, efficient neuronal/cell uptake, better brain accessibility, sustained release, and desired therapeutic effect. The *in-silico* studies were performed to determine the target proteins/sites and stipulate the possible mechanism of action of the DPL-EMB combination. Cell line studies were further conducted to assess the drug cytotoxicity and determine the combination ratio with maximum effective synergism. DPL-EMB NLCs were synthesized via a hot emulsification sonication technique and were optimized by implementing a Central composite rotatable design (CCRD). The physicochemical characteristics of combinatorial NLCs were ascertained through the utilization of Differential scanning calorimetry (DSC), Fourier-transform infrared spectroscopy (FTIR), transmission electron microscopy (TEM), and scanning electron microscopy (SEM). NLCs were further assessed for particle size, particle-size distribution, zeta potential, drug entrapment, drug loading, *in vitro* release, and *ex vivo* permeation in the goat-excised nasal mucosa. Moreover, histopathological studies, DPPH assay, HET-CAM assay, and cellular uptake studies have also been performed.

2. Materials and methods

2.1. Materials

DPL and EMB were acquired from **Sun Pharma Research Lab (Gurgaon, India)** and Sigma-Aldrich (St. Louis, USA), respectively. Stearic acid, Oleic acid, Black seed oil, Castor oil, Tween 80, and Tween 20 were obtained from SD-fine Chemicals, Ltd. (Mumbai, India). Compritol 888 ATO, Precirol ATO5, Gelucire, Geleole, Thymoquinone, Capryol 90, Cremophore EL, Solutol HS 15, and Poloxamer 407 were acquired from Gattefose India Pvt. Ltd., Mumbai, India. All the additional chemicals were procured from Northern laboratory implements, Sigma-Aldrich, and SD Fine Chemicals, India. Milli-Q grade water (Millipore, Molsheim, France) was utilized for the study. The chemicals employed for fabricating NLCs were analytically graded.

2.2. DPL-EMB compatibility studies

DPL and EMB were precisely weighed and combined in a 1:1 ratio. The mixture was then stored in a vial for 28 days at $40 \pm 2^\circ \text{C}$ and $75 \pm 5\% \text{RH}$ in a stability vessel. The physical incompatibility of the drugs was evaluated visually for any signs of caking, liquefaction, discoloration, precipitation, opalescence, odor, or gas generation. FTIR and DSC spectrum analysis was then used to evaluate relevant chemical interactions. Pellets were made by combining KBr and sample in a ratio of 100:1, and infrared spectra of the sample were recorded using an FTIR spectrometer. The dried sample of a mixture (1:1) was firmly sealed into an aluminum pan using a DSC loading puncher. Using a Pyris 6 DSC differential scanning calorimeter, the sample was heated to between 50 and 4000 C at 50 C/min while immersed in a nitrogen atmosphere. (USA, Perkin Elmer, CT).

2.3. In silico study

Protein Data Bank contained the three-dimensional structure of AChE (PDB ID1B41). The SMILES strings were acquired from PubChem, National Centre for Biotechnology Information (NCBI), and imported into the molecular modeling simulation software Auto Dock to create the 3D structure of smaller molecules. Based on the existing literature, the catalytic site of AChE was determined. The catalytic residue was further analyzed using Q-Site Finder. Q-Site Finder analyzes the interaction potential between an amino acid and van der Waals probe to identify energetically active pockets. AutoDock was used to determine the docked complex's fundamental interactions and interaction energies. The 3D coordinates of the AChE and inhibitor/substrate (DPL and EMB) were provided in PDB format with default values. Significant H atoms, solvation forces, and Kollman and Gasteiger charges were encompassed using AutoDock tools. Using the Autogrid application, the grid points and distances were created [29]. Utilizing AutoDock's dielectric operations, the Van der Waals and electrostatic parameters were calculated. The Lamarckian genetic algorithm (LGA) and the Solis & Wets local search approach were used to simulate docking [30]. Each experiment comprised ten runs programmed to cease after a maximum of two million and fifty thousand energy assessments. The population was restricted to 150 individuals. The torsion, translational, and quaternion steps of 5 were applied during the search. EMB, a multi-faceted molecule with different mechanisms of action, was further docked to $\text{A}\beta$ (Amyloid beta protein) active sites (monomers and fibrils).

2.4. Cell line studies

2.4.1. MTT Assay for cell viability

N2a, a rodent neuroblastoma cell line, was employed. The cells were cultured in a humid setting with 5% CO_2 at 37°C until they converged. The culture medium used was minimum essential medium (MEM) enriched with 10% (v/v) fetal bovine saline (FBS), penicillin (100 IU/ml), streptomycin (100 mg/ml), and

amphotericin B (5 mg/ml). Subsequently, the cells were transferred into 96 array culture plates in preparation for the experiment. The cytotoxicity assay was carried out using cell suspension, containing 10,000 cells seeded in each well of a 96-well microtiter plate (Nunc and Tarsons, Kolkata, India) and incubated for 24 h at 37 °C. After treatment with drugs, i.e., DPL and EMB separately (24 Hrs), the medium was removed, and N2a cells were incubated with fresh medium containing MTT (Sigma, St. Louis, MO; 0.9 mg/ml final concentration) for 2 h at 37 C. MTT, i.e., 3-(4, 5-dimethyl thiazolyl-2)-2, 5-diphenyltetrazolium bromide (Orange color) is converted to Formazan (Purple color) by the living cell's mitochondrial reductase enzyme. This conversion, thus, is an indication of viability. Isopropanol and Sodium dodecyl sulfate (20%) was introduced and allowed to incubate for 20 minutes to facilitate the extraction of the Formazan produced, which was subsequently assessed at 560 nm using a plate reader. The more viable cells, the more the purple color's conversion, and intensity. IC50 value, i.e., the concentration of a compound that exhibits 50% inhibition, was determined for DPL and EMB separately. The duplicate reading for each sample was arranged, medium culture background was subtracted from assay readings to give corrected absorbance. % Cell cytotoxicity was estimated as-

%Cell cytotoxicity = $100 \times (\text{control-sample})/\text{control}$

2.4.2. Determination of Synergism effect or Combination Index

A 96-well microtiter plate was seeded with 10,000 N2a cells per well, treated with 10% FBS, and maintained for 24 hours at 37°C in an environment with 5% CO₂. Following a 24-hour incubation period, the cells were subjected to a combination of DPL and EMB samples at varying ratios (namely, 1:1, 1:2, 1:3, 1:5, 1:7, and 1:10), where the concentration of DPL remained constant, and the concentration of EMB was adjusted relative to the IC50 concentration. Consequently, an MTT test was conducted to determine the potential cytotoxic effects. The study utilized Compusyn 1.0 version software to determine the combination index (CI) and define the observed effects as synergistic (CI < 1), additive (CI = 1), or antagonistic (CI > 1).

2.5. Screening of Excipients

2.5.1. Screening and selection of solid lipid

The solubility of DPL and EMB in numerous solid lipids (Stearic acid, Compritol ATO 888, Precirol ATO 5, Geleole, and Gelucire) was determined by incorporating the iterative amount of drug (5mg) to 1g of molten solid lipid (heated to 20°C above the melting point) until no further dissolution occurred. DPL and EMB solubility in molten solid lipids were determined. The experiment was repeated three times [31].

2.5.2. Screening and selection of liquid lipid

By adding excess quantities of the drugs, one at a time, to 1ml liquid lipid in vials containing oleic acid, castor oil, black seed oil, thymoquinone, and Capryol 90, the solubility of DPL and EMB was assessed in liquid lipids. The vials were sealed and mechanically shaken continuously at 25.0 ± 0.5°C for 72 hours to achieve equilibrium. High-speed centrifugation at 12000 rpm of the mixtures was performed for 30 minutes. The supernatant was separated and diluted with methanol, and the absorbance was measured in triplicate at λ_{max} 229 nm (for DPL) and λ_{max} 294 nm (for EMB) using a UV spectrophotometer [31].

The physical compliance of the chosen liquid and solid lipids was also examined. The solid-to-liquid lipid mixture (1:1) in a glass tube was heated to 70°C and cooled before congealing. Layer separation in a cooled congealed lipid mass was an indicator of incompatibility visually examined in the binary combination under bright light [32].

2.5.3. Selection of solid lipid to liquid lipid ratio

The miscibility between solid lipid and liquid lipid with the maximum solubility for DPL and EMB was assessed for solid-to-liquid lipid combination ratios of 90:10, 80:20, 70:30, 60:40, and 50:50. The binary composition was swirled for 1 hour at 200 rpm at 85°C, cooled to room temperature, and applied onto filter paper. The presence of oil droplets on the filter paper was visually inspected, and the mixture with a melting point over 40°C and no oil droplets on the filter paper was chosen for the synthesis of DPL and EMB-loaded NLC [31].

2.5.4. Screening and selection of surfactant

The capacity of the surfactants (Polaxamer 407, Tween 20, Tween 80, Cremophore EL, and Solutol HS 15) to emulsify the binary mixture led to their selection. 100 mg of the binary combination was dissolved in 3 ml of methylene chloride, followed by 10 ml of a 5 percent (w/w) aqueous solution of various surfactants while maintaining the same temperature. The resulting liquid was heated to 40°C and stirred using a magnetic stirrer to remove the additional methylene chloride. Then, using a UV spectrophotometer, the % transmittance of the diluted combination at 510 nm was measured in triplicate using 1 ml of this mixture diluted with 10 ml of distilled water [33].

2.6. Experimental design

Quality by design (QBD), a methodical strategy based on developing both product and process and control and quality risk management (ICH Q8), was followed for developing NLCs. A sequential flow of the approach was trailed as-

- Specified the Target product profile (TPP) and the Quality target product profile (QTPP)
- Identified critical quality attributes (CQAs)
- Identified critical material attributes (CMAs) and critical process parameters (CPPs)
- We assessed the effect of CMAs and CPPs on CQAs via Ishikawa or cause and effect investigation.
- Conducted a risk assessment by linking together CMAs and CPPs and assessed their effect on failure modes via the Failure mode effect analysis method (FMEA)
- Generated design space

- Depicted control strategy
- Life cycle management and continual improvement

2.7. Drug-Excipients (D-E) compatibility study

The drugs (DPL and EMB), lipid mixture (Stearic acid and Capryol 90), and surfactant were weighed and precisely combined. The mixture was then stabilized in a vessel for 28 days at $40 \pm 2^\circ\text{C}$ and $75 \pm 5\%$ RH. The interaction between the active ingredients and excipients was visually evaluated for any physical incompatibility, such as caking, liquefaction, discoloration, precipitation, opalescence, odor, or gas production. In addition, the D-E compatibility was investigated by performing DSC and FTIR analysis on the optimized formulation to identify any potential chemical interactions between the drugs, lipid mixture, and surfactant.

2.8. Optimization and fabrication of DPL-EMB NLCs

2.8.1. Preparation of DPL-EMB NLC for intranasal delivery

The hot emulsification sonication technique was applied to produce DPL-EMB NLCs. The binary combination of stearic acid and Capryol 90 was made in an optimal ratio (7:3). DPL and EMB were dissolved in the binary mixture and melted at 70°C (lipid phase). 1ml of water was then incorporated in the lipid phase at 500 rpm at 80°C . Tween 80 was dissolved in 9 mL of distilled water at 500 rpm and 80°C to produce the aqueous phase. The lipid phase was maintained at a constant temperature while the aqueous phase was gradually added dropwise at 800 rpm. Using the probe sonicator, the resulting emulsion was sonicated for one minute (Hielscher, Germany). The resulting NLC formulations were put through evaluation testing.

2.8.2. Optimization of dual drug-loaded Nanostructured Lipid Carrier using CCRD

To determine the impact of a binary mixture of lipids (BML) concentration, surfactant concentration, and sonication time on the particle size, zeta potential, polydispersity index (PDI), % drug loading, and % entrapment efficiency (EE), central composite rotatable design (CCRD) via Design Expert 13.0.2.0 (Stat-Ease, Minneapolis) was used. Table 1 displays the bounds of the independent factors. The spectrum of independent variables was selected based on preliminary trials. The table below describes the design set up of various runs produced by the software. Twenty of the formulas recommended by the software were developed.

Table 1
Independent factors considered for CCRD

Factors	Levels	
	Low	High
Independent factors		
A = Lipid concentration (%w/v)	1	3
B = Surfactant concentration (%w/v)	2	5
C = Sonication time (sec)	40	120
Dependent factors	Restraint	
R1 = Mean particle size (nm)	Minimum	
R2 = PDI	Minimum	
R3 = % Entrapment efficiency	Maximum	

3. Characterization of DPL-EMB loaded NLCs

3.1. Surface Morphology

Transmission electron microscopy (TEM; Morgagni 2680, Massachusetts, USA) examination was used to assess further the particle size and shape of the optimized DPL-EMB NLCs. In order to assist the optimized NLC stick to the carbon substrate, samples were diluted approximately 50 times with distilled water before adding, instilling it onto the grid, and retaining it for one minute. Phospho-tungstate (1%) was applied, and the grid was positioned on it prior to the filtration of the leftover solution. Subsequently, the samples underwent desiccation and were scrutinized via transmission electron microscopy (TEM). Every analysis was conducted in triplicate [34].

Scanning electron microscopy (SEM; Leo 435 VP) was used to analyze the surface morphology of optimized DPL-EMB NLCs. The sample was applied as a tiny drop to a rectangle glass stub and air-dried for SEM. NLCs were examined by scanning electron microscopy after the dried thin film of NLCs was coated with gold using a glass sputter casting method in a high vacuum vaporizer to make it conduct [35].

3.2. Particle size, polydispersity index (PDI), and zeta potential (ZP)

The particle size (diameter) and the PDI of combinatorial DPL and EMB NLCs were determined using a zeta sizer (Malvern Instruments, UK). Milli Q was used to dilute the NLC dispersion in the ratio of 1:100. Water, used as a dispersant, had viscosity and refractive index of 0.9 cP and 1.3 at $25 \pm 2^\circ\text{C}$, respectively [36].

Electrophoretic light scattering with Delsa Nano C was used to assess the ZP of optimized DPL-EMB NLCs (Beckman Coulter). To evaluate the zeta potential, 1mL of the sample was obtained and diluted 10 times. Helmholtz-Smoluchowski equation converts particle velocity to zeta potential based on Doppler

phenomena [37].

3.3. Entrapment efficiency and drug loading

By passing the synthesized NLCs through Millex filters (0.22 µm) (Millipore, US), residual insoluble compounds were removed. In one liter of methanol, prepared NLC was dissolved. Quantifying the concentration or amount of both drugs in NLC was done using the validated UV simultaneous estimation method (C_{total}). The NLCs underwent vortexing for 5 min and spun for 30 min at 12,000 rpm to segregate the non-enveloped drug from the enveloped drug. The supernatant was analyzed to determine the concentration of the non-enveloped drugs (C_{free}). %EE and drug loading of DPL and EMB in dried and weighed NLC was calculated as:

$$\%EE = (C_{total} - C_{non-enveloped})/C_{total} \times 100$$

$$\text{Drug loading (\%)} = (C_{total} - C_{non-enveloped})/WNLC \times 100$$

3.4. FTIR and DSC analysis

The infrared spectrum of a lyophilized sample of optimized DPL-EMB NLCs was taken using a hundred parts of potassium bromide (KBr) and one part of the sample, and then pellets were made. FTIR spectra of the sample were recorded using an FTIR spectrometer to analyze any chemical interaction between the drug, surfactant, and lipids.

Pyris 6 DSC (Perkin Elmer, USA) was implied to thermally scrutinize the NLC formulation and bulk materials to examine drug, surfactant, and lipid interactions and solid lipid polymorphism. The structural characteristics of NLC, demonstrating whether it is amorphous or crystalline, were also demonstrated using DSC. Before performing DSC, the NLC formulation was freeze-dried and lyophilized. In aluminum pans, dried samples weighing about 5 mg were fully sealed. An aluminum pan that had been emptied was used as a reference. Samples were heated at 10°C/min within a nitrogen setting at 25 to 300°C temperatures. The samples' crystallinity index (CI) was obtained using enthalpy values considering stearic acid as the main solid lipid component by the equation-

$$\%CI = \Delta H_{NLC}/\Delta H_{Solid\ lipid} \times 100$$

ΔH_{NLC} and $\Delta H_{Solid\ lipid}$ indicate the DPL-EMB NLCs and stearic acid enthalpy values, respectively.

3.5. *In Vitro* Drug Release and Release Kinetic Study

The release of drugs from optimized DPL-EMB NLCs was assessed via the dialysis bag technique. The dialysis membrane's (12,000–14,000 Da) (Himedia) glycerin was eliminated by washing it under running water for three to four hours, and the Sulphur compounds were eliminated by treating them with a 0.3 percent sodium sulfate (w/v) at 80°C for one minute. The tube was subjected to hot water to eliminate the sulfuric acid after being rinsed for 2 minutes. Most proteins with a molecular weight of 12000 or more were retained by membranes after this treatment. For activation, the dialysis membrane was immersed overnight in phosphate buffer solution (PBS 7.4) [37]. DPL and EMB were released from NLC and deferred in Phosphate Buffer Saline (PBS, pH 7.4). The dialysis bag traps nanoparticles and permits the entry of free drugs into the dissolving medium [38]. The dialysis tube's membrane was secured using thread. Optimized DPL-EMB NLCs and suspension were transported to different assemblies of dialysis tubes. Phosphate-buffered saline (PBS) solution with a pH of 7.4 was utilized alongside a dialysis tube under continuous stirring at 100 revolutions per minute at 37 ± 100 ° C. Fractions of the sample were collected from the receptor compartment at specified time intervals, and the volume was adjusted using PBS. Samples were analyzed at each time point using UV spectrophotometry at 229 nm and 330 nm to estimate the levels of DPL and EMB simultaneously. The experiment was performed thrice, and the mean cumulative percentage of drug release and its corresponding standard deviation were used to present the findings. The release mechanism was established by modeling in vitro release values in multiple drug release kinetics (Zero order, first order, Higuchi, Korsmeyer Peppas model, etc.).

3.6. DPPH ASSAY

At room temperature, the optimized DPL-EMB NLCs were tested against 2, 2-diphenyl-1-picrylhydrazyl (DPPH), an antioxidant. Antioxidant assay methods include the DPPH free radical technique. The ability of antioxidants to scavenge electrons caused the violet-colored solution of the DPPH free radical at room temperature to turn colorless when it reacted with any antioxidant molecule. The sample's antioxidant effectiveness was also assessed using spectrophotometric analysis of the color change. At room temperature, DPPH free radical solution in ethanol was used to treat the samples that would be analyzed. After being dissolved in 3 ml of methanol, 0.5 ml of the sample was treated with 0.3 ml DPPH methanolic solution (0.3 mM). Due to the samples' ability to donate hydrogen, the color resulting from the reaction was measured to determine its antioxidant potential following 100 minutes of reaction in a dark environment by calculating the reaction mixture's UV absorbance at 517 nm. The control solution comprised methanol and DPPH solution measured at 3.5 ml and 0.3 ml, respectively, whereas the blank solution comprised 3.3 ml methanol and 0.3 ml sample. Samples' capacity to scavenge free radicals was expressed as a percentage of Ascorbic acid [39].

3.7. *Ex vivo* studies

3.7.1. Preparation of goat nasal mucosa

After an animal sacrifice, a goat nose was obtained from a nearby slaughterhouse. A longitudinal incision with a blade was used to delicately peel out the whole nasal mucosa from the anterior margin of the nose. In order to conduct a permeation investigation and confocal imaging assessment, the separated nasal mucosa was cleaned twice or three times with distilled water, preserved in a 10 percent v/v formalin solution, and placed in the freezer at minus 20°C [37].

3.7.2. *Ex vivo* permeation investigation on the nasal mucosa

Ex vivo investigations were carried out utilizing the Franz cell with a cross-sectional area and capacity of 1.76 cm² and 10 ml, respectively, to determine how effectively DPL-EMB-loaded NLC permeates through the nasal mucosa. Goat nasal mucosa that had just been removed was collected in Nasal Saline Buffer (NSB), pH 6.4 [37]. The upper segment of the nasal membrane was excised, dissected, and positioned within the Franz diffusion apparatus, interposed between the donor and receiver cells, with the mucosal part centered on the donor cell. The tissue was subjected to stabilization prior to magnetic stirring for 15 minutes in NSB pH 6.4. The thermostat for the diffusion cell was set to 37 ± 0.5 °C. After 15 minutes, the solution from both cells was withdrawn, and NSB was freshly added to the receiver. In order to prevent diffusion media leakage, the diffusion cell's donor cell was positioned over the nasal membrane mounting and clamped to the lip of the receiver cell. By depositing 2 ml of the samples onto stabilized sheep nasal membrane in the donor cell of the Franz diffusion assembly and constantly stirring at 100 rpm, permeation investigations of DPL-EMB loaded NLCs and DPL-EMB suspension were conducted [40]. At predefined time intervals, aliquots (0.5 ml) of the receiver cell were withdrawn, filtered using nylon filter paper (0.45 mm), and then subjected to UV analysis at 229 nm and 334 nm. Each sample that was taken was promptly substituted with an equivalent quantity of diffusion medium that was kept at 37 ± 0.5 °C. At each sampling site, the amount of DPL and EMB traversed through the sheep nasal mucosal barrier was estimated using the simultaneous estimation method by UV. Permeation profile was obtained by plotting drug permeation per unit surface area of the nasal membrane (µg/cm²) against time (h). The steady-state flux, J_{ss} (µg/cm²/h), was deduced using linear regression analysis from the slope of the curve. The results of each measurement were repeated three times.

3.7.3. *Ex Vivo* confocal laser scanning microscopy (CLSM) visualization

Stacked rhodamine B dye DPL-EMB suspension and an optimized DPL-EMB NLC formulation were produced. Rhodamine-loaded NLCs, suspension, and methanolic solution of rhodamine were employed as the test substances and stabilized nasal mucosa with NSB (PH 6.4) as control. The cleaned mucous membrane was sliced into small segments and rinsed with distilled water to form a microscopic slide. To evaluate the penetration of optimized NLCs and suspension in the entire mucosal layers, the produced slides were examined using CLSM (Leica TCS SPE, UK) [41]. Rhodamine fluorescence was optically activated for this investigation using Argon irradiation, and photoluminescence above 532 nm was measured.

3.7.4. Nasal histopathological studies

Nasal histological examinations were conducted using goat nasal mucosa freshly obtained from a slaughterhouse and preserved in a nasal saline buffer (NSB, pH 6.4). Each piece of tissue was subjected to DPL-EMB suspension, Opt DPL-EMB NLC, Nasal saline (pH 6.4), and a nasal mucociliary toxicity agent, i.e., isopropyl alcohol, respectively. Following a two-hour treatment period, every sample underwent cleansing, sectioning, and staining with hematoxylin and eosin. After removing the mucosa, the mucociliary was studied under an optical microscope.

3.8. Hen's Egg Test-Chorioallantoic Membrane (HET-CAM) Assay

Pure white fertilized leghorn chick eggs were bought from a Poultry farm in Gurgaon, Haryana, India. When eggs arrived at the lab, the shells were examined for breakage, and damaged eggs were rejected. Unaffected eggs were incubated at 37 ± 0.2 °C and 40 ± 2% relative humidity. Aseptically drilling the eggshell removed albumin (2–3 ml). Using a heated spatula and 70% alcohol-sterilized parafilm, the hole was sealed that day before the eggs were placed in the equatorial orientation for incubation. The test samples were immediately injected onto the CAM surface on the tenth day via an appropriate opening, where they were then allowed to come into contact for 5 minutes. 0.9% NaCl and 0.1 N NaOH were employed as a negative and positive control, respectively. The test formulations used were drug suspension and optimized DPL-EMB-loaded NLC. In the experiment, each group received eight eggs. Each sample's irritating response was assessed by keeping track of three endpoints for five minutes each: coagulation, lysis, and hemorrhage. The outcomes were assessed using irritation scores (IS), with a range of 0 to 0.9 regarded as non-irritant, 1 to 4.9 as marginally irritant, 5 to 8.9 as mildly irritant, and 9 to 21 as highly irritant. Over ten minutes, the effects were continually observed, and the moment the irritation began was noted. When the assays were completed, images were taken, application of the following equation to the calculation of the IS [42].

$$[(301\text{-Hemorrhage time}/300) \times 5] + [(301\text{-Lysis time}/300) \times 7] + [(301\text{-Coagulation time}/300) \times 9]$$

Times should be substituted with the start time (in seconds) for each effect.

3.9. Cellular uptake studies by Transmission Electron Microscopy

To investigate the uptake of optimized DPL-EMB-loaded NLCs by N2a cells, cells were seeded at a density of 10⁵ cells/cm² in 25 cm² cell culture flasks and allowed to grow for 24 hours (37 °C, 5% CO₂). Subsequently, cells were treated with DPL-EMB NLCs for 24 h in culture augmented with FBS (10% v/v), penicillin (100 IU/ml), streptomycin (100 mg/ml), and amphotericin B (5 mg/ml) in a humid chamber with 5% CO₂ at 37 °C. After NLC incubation, the cells were dislodged and centrifuged to create a pellet. The cells were delicately washed and resuspended in PBS before being transferred to standard copper TEM grids and observed using a transmission electron microscope (TEM, Morgagni 2680, Massachusetts, USA).

3.10. Stability Study

Stability investigations were performed to ascertain the reliability of the composition throughout its shelf life. Accelerated stability assessments of OPT-DPL-EMB NLC were conducted for a duration of three months as per the norms set forth by the International Council for Harmonization (ICH) in Q1A R2. The study observed the influence of elevated temperature, i.e., 40 ± 2 °C and 75 ± 5% RH, on the stability of the formulation at 0, 1st, 2nd, and 3rd month. The formulations regarding standards for determining colloidal system stability were evaluated, including Particle size, PDI, ZP and % EE.

4. Results and Discussion

4.1. DPL-EMB compatibility studies

Visual inspection of the mixture of DPL and EMB (1:1) sustained at $40 \pm 2^\circ\text{C}$ and $75 \pm 5\%$ RH in a stability vessel for 28 days showed no visible change in both compounds' Organoleptic properties (Table 2). Moreover, the FTIR graph (Fig. 2B) revealed distinctive bands of absorption at 1686 cm^{-1} for conjugation keto moiety and $1591, 1500,$ and 971 cm^{-1} for arenes for DPL and characteristic bands at 1613 cm^{-1} for conjugation keto moiety, 1193 for C-O bond, 3311 for O-H bond, 2861 for C-H bond and 2922 cm^{-1} for aromatic C-H for EMB. Also, the DSC thermogram (Fig. 2A) of the mixture revealed no notable interaction between DPL and EMB; however, due to the presence of EMB, there was an imperceptible deprivation in DPL's melting point. Thus, no significant interaction between the two compounds was evident.

Table 2
DPL-EMB Compatibility (Visual observation)

Drug/Mixture	Visual observation ($40 \pm 2^\circ\text{C}$ & $75 \pm 5\%$ RH, 28 days)					
	Caking	Liquefaction	Discoloration	Precipitation	Opalescence	Odor/Gas formation
DPL	No	No	No	No	No	No
EMB	No	No	No	No	No	No
DPL + EMB	No	No	No	No	No	No

4.2. In silico study

The findings of docking investigations are denoted by the measure of interaction in negative kilocalories per mole. The docked configurations of DPL and EMB and significant interactivities are given in Table 3, and 2D and 3D images of docked molecules to their respective target sites are shown in Fig. 3. Based on the results of the docked configurations of EMB and A β , binding to fibril 5A β_{17-42} displayed high interaction energy of -38.8011 when compared with A β monomers.

Table 3

Key Interactions and interaction energy of EMB and DPL docked to active sites of A β (Monomers/Fibrils) and Acetylcholinesterase (AChE)

Drug	PDB ID (Target site)	Interaction Energy (-kcal/mol)	Interactions
EMB	1BA4 (A β 1-40)	34.2101	Hydrogen Bonds
			EMB to ASH1
			Hydrophobic associations
			EMB to PHE20
			EMB to VAL24
			EMB to ALA21
			EMB to LEU17
			EMB to VAL12
			EMB to TYR10
			Electrostatic interactions
			EMB to GLU11
			EMB to GLU3
			EMB to ASP7
			EMB to LYS16
			EMB to ARG5
EMB to GLN15			
EMB to HIS14			
EMB to SER8			
EMB	2BEG (5A β 17-42)	38.8011	Hydrogen Bonds
			EMB to ILE41
			Hydrophobic associations
			EMB to VAL40
			EMB to VAL39
			EMB to LEU17
			EMB to VAL18
EMB to PHE19			
EMB	4EY7 (AChE)	65.7525	Hydrogen Bonds
			EMB to ARG296
			EMB to PHE295
			Hydrophobic associations
			EMB to PHE297
			EMB to TYR341
			EMB to TYR337
			EMB to TYR338
			EMB to LEU289
			EMB to TRP286
			EMB to ILE451
			EMB to VAL294
			Electrostatic interactions
EMB to ASP74			

			EMB to GLU202
			EMB to THR83
			EMB to HIS447
			EMB to SER293
DPL	4EY7 (AChE)	48.5319	Hydrogen Bonds
			DPL to PHE295
			π - π stacking
			DPL to TRP286
			DPL to TRP86
			Salt bridge
			DPL to ASP74
			π -cation interactions
			DPL to PHE338
			DPL to TRP86
			Hydrophobic associations
			DPL to VAL294
			DPL to PHE297
			DPL to TYR124
			DPL to TYR337
			DPL to ILE451
			Electrostatic interactions
			DPL to HIS447
			DPL to THR83
			DPL to SER293
			DPL to SER125
Superimpose docked pose (DPL+EMB)	4EY7 (AChE)	-	Hydrogen Bonds
			EMB to PHE295
			EMB to ARG296
			DPL to TYR337
			DPL to TYR341
			π - π interaction
			DPL to TRP86
			π -cation interaction
			DPL to PHE338

However, EMB has been reported to interact with other active sites of A β ; the rationale for selecting these two target sites for the molecular docking study of EMB was the drug's better binding affinity (higher interaction energy) with functional pockets in the light of prior literature. The results concurred with a similar study by Bhuvanendran et al., indicating that EMB has an optimal binding state within the active sites of the A β peptide. Furthermore, it was observed that EMB exhibited superior binding affinity to the active site of AChE, as evidenced by its interaction energy of -65.75 kcal/mol, in comparison to DPL, which is also an inhibitor of AChE. This finding exhibited conformity with the acetylcholinesterase inhibitory attributes of EMB. Hence, based on this study, we discovered that EMB is a favorable compound that can be further developed into a potential therapeutic multipotent agent for AD [26]. The hydrophobic interactions of EMB and DPL with their respective targets, as given in Table 3, indicated a high degree of lipophilicity of both the drugs, which would ultimately make it feasible for the drugs to pass through hydrophobic channels within the brain and target proteins and provide the desired pharmacological effect.

Higher binding interaction energy indicated that EMB might bind to the A β active sites and AChE, likely triggering the catalytic site for its inhibitory activity for A β and AChE [25]. The synergistic approach of combining DPL and EMB for the treatment of AD was further supported by the obtained docking results, which stipulated a common mechanistic pathway being followed by both the drugs; that is, they both bind effectively to AChE with the interaction energies of -48.5319 and -65.7525 respectively. Figure 3K describes the superimpose docked pose of DPL and EMB to the AChE (DPL light green stick model and EMB turquoise stick model), red colored dashed line show hydrogen bonding interactions, turquoise-colored dashed lines show π - π interactions and green colored dashed lines show π -cation interactions between the drugs and binding sites of AChE. The critical interactions of the superimpose docked pose are provided in

Table 3. Also, DPL and EMB are bound to AChE but at different sites, indicating the absence of competition for the same binding site between the drugs. These results proved that a prompt and robust AChE inhibition could be attained via combination therapy (Synergistic effect).

4.3. Cell line studies

4.3.1. MTT Assay for cell viability

The N2a cell viability for DPL (24 Hrs) is shown in Fig. 4B. The calibration plot between the concentration and % cell death (%cytotoxicity) (Fig. 4A) revealed the IC50 concentration of DPL as 979.9 nM. The N2a cell viability data for EMB (24 Hrs) is shown in Fig. 4D. The calibration plot between the concentration and % cell death (%cytotoxicity) (Fig. 4C) revealed the IC50 concentration of EMB as 54.5 μ M.

4.3.2. Combination index or synergistic effect

Compared to ratios 1:3, 1:5, 1:7, and 1:10 at lower concentrations, ratio 1:1 produced the highest N2a cell viability in 24 hours (Fig. 5A). Compusyn 1.0 was employed to compute the combination index (CI), which advised a 1:1 ratio of DPL and EMB for drug combination studies to have the greatest possible synergistic effect (CI was found to be 0.189). (Table 4). Figure 5B, C, and D display the dose-effect curve, the combination index plot, and the logarithmic combination index plot. Data, therefore, suggested that NLC formulations be developed with a 1:1 drug combination ratio for the N2a cell line.

Table 4

CI values for actual experimental points		
Drug Combination (DPL+EMB)	Fa (Effect)	CI Index
1:1	0.45	0.189
1:3	0.43	0.36
1:5	0.41	0.513
1:7	0.35	0.583
1:10	0.18	0.456

4.4. Screening of Excipients

4.4.1. Screening and selection of solid lipid

The DPL and EMB solubility data in different molten solid lipids are shown in Fig. 6A and B, respectively. According to the solubility results, DPL and EMB both demonstrated higher solubility in stearic acid due to a hydrogen bonding between the drugs and the carboxylic acid functional group of stearic acid as the dominant factor [43]. Non-polar dispersion and π - π bond interactions can also contribute to the solubilization of APIs. Additionally, Choi et al.'s DPL in vitro permeation investigation revealed a parabolic relationship between fatty acid carbon-chain lengths and permeation amplification. The most effective increase in DPL penetration rate among saturated fatty acids with 12 to 20 carbon units was stearic acid (C18) [44].

Additionally, stearic acid can shield cortical neurons from oxidative stress by increasing the internal antioxidant enzymes (Cu/Zn SOD and CAT) and reducing lipid peroxidation. The primary activation of PPAR γ and subsequent synthesis of proteins in cortical neurons mediates the neuroprotective effect [45]. This will provide the formulation with enhanced therapeutic value. Stearic acid was thus selected based on the above findings.

4.4.2. Screening and selection of liquid lipid

The solubility of DPL and EMB in various liquid lipids measured by the UV spectrophotometric method is displayed in Fig. 6C and D, respectively. Based on the solubility results, DPL and EMB showed higher solubility in Capryol 90. Moreover, liquid lipid Capryol 90 acts as a co-emulsifier due to its surface-active properties (HLB = 6), leading to small particle size and narrow particle size distribution (PDI \approx 0.13), yielding stable NLCs suitable for intranasal delivery [46].

4.4.3. Selection of solid lipid to liquid lipid ratio

Different ratios of solid-to-liquid lipids were analyzed visually for the occurrence of oleaginous spots on the Whatman filter, and a 70:30 ratio was selected. No sign of layer separation in cooled congealed lipid mass (Binary mixture) was visualized, indicating compatibility between liquid lipid and solid lipid.

4.4.4. Screening and selection of surfactants

The surfactant selection was based on the emulsification potential, and tween 80 showed maximum transmittance (Fig. 6E). Moreover, Tween 80 has been reported as a P-gp efflux inhibitor [47], impeding the efflux of DPL (P-gp substrate). Tween 80 has also been reported to enhance nasal permeation of drugs through nasal mucosa [48]. Based on the above findings, tween 80 was chosen as a surfactant.

4.5. Experimental design

The various QTPP components and their rationales have been compiled to construct NLCs (Table 5). Justification for the selection of CMAs and CPPs is displayed in Table 6. Ishikawa diagram representing the effects of CMAs and CPPs on CQAs of DPL and EMB-loaded NLCs is shown in Fig. 7. Various Risk factors and the effect of CMAs and CPPs on failure modes are illustrated in Table 7

Table 5
QTPP with their justification for NLC development

QTPP	Target	Justification
Formulation	NLCs	The liquid dosage form is well suitable for the intranasal route of delivery.
Drug release pattern	Controlled release	Including controlled release characteristics has been shown to enhance the degree of drug absorption and foster a sustained effect.
Administration route	IN	IN route optimal approach for administering drugs in the management of cerebral conditions. (Bypassing BBB)
Particle size	< 200 nm (CQA)	According to published research, particles smaller than 200 nm are preferred to achieve optimal permeation of drugs through nasal membranes and cellular uptake via a variety of mechanisms depending on particle size, including receptor-mediated endocytosis for particles between 50 and 120 nm, clathrin or caveolin-mediated endocytosis for particles between 120 and 200 nm and phagocytosis for particles between 250 and 3000 nm [49].
PDI	< 0.5 (CQA)	Poly-dispersed systems tend to form aggregates; thus, the moderately dispersed system having lower PDI is desirable to achieve a stable particulate system.
ZP	~ 30 mv (CQA)	To render NLC formulations more resilient since electrostatic tension between nanoparticles precludes agglomeration.
% EE	> 80% (CQA)	A higher entrapment efficiency is desired to deliver the therapeutic dose for clinical efficacy and to obtain sustained release.

Table 6
CMAs and CPPs selection with their justification

Drug attributes (CMA)		
Drug	Justification	
DPL	The intranasal administration of NLCs presents a clinically intriguing strategy for augmenting brain efficacy while mitigating toxicity to non-target organs.	
EMB	The nanosizing of particles can overcome the low solubility problem.	
Excipients attributes (CMA)		
Excipients	Justification	
Selection of solid lipid	Stearic acid	Stearic acid was chosen based on parameters like solubility, permeation enhancement, and neuroprotective effects on Alzheimer's disease.
Selection of liquid lipid	Capryol 90	Capryol 90 was selected based on parameters like solubility, permeation enhancement, and its co-emulsifying properties resulting in smaller particle size and narrow PDI.
Selection of surfactant	Tween 80	Tween 80 was selected for the determined binary combination of solid and liquid lipids based on their emulsification potential.
Critical process parameters (CPP)		
Process	Justification	
Sonication time	30 sec-120 sec	Trial batches were used to determine the sonication time. However, prolonged sonication was avoided due to drug leaking from the matrix and lipid globule agglomeration.

Table 7
Failure mode effect analysis (FMEA)

Risk factors	CMAs	CPPs	Failure modes
Particle size	Surfactant type and concentration, Conc. of Lipid mixture, solid to liquid lipid ratio	Sonication time, temperature, and amplitude	Change in content uniformity, <i>in-vitro</i> drug release, and <i>ex-vivo</i> nasal permeation.
Entrapment efficiency	Surfactant and binary mixture concentration.	Sonication time and temperature	Change in the dose and content uniformity of the drug, change in release pattern.
Zeta potential	Surfactant type and conc.	Sonication time.	Change in formulation stability and aggregation of particles possible.
PDI	Surfactant and lipid conc.	Sonication time.	Aggregation of particles may lead to a poly-dispersed system which affects stability.

4.6. Drug-Excipients (D-E) compatibility study

Visual inspection of the mixture of DPL and EMB with Excipients (Stearic acid, Capryol 90, and Tween 80) kept at $40 \pm 2^\circ\text{C}$ and $75 \pm 5\%$ RH in a stability chamber for a period of 28 days showed no visible change in the Organoleptic properties of both the compounds (Table 8). Further, the DSC and FTIR results of the optimized NLC formulation would provide evidence of any physical or chemical interaction between the drugs and excipients.

Table 8

Drug-Excipient interaction study (Visual Observation)

Drug Excipients Mixture	Visual observation (40 ± 2°C & 75 ± 5% RH, 28 days)					
	Caking	Liquefaction	Discoloration	Precipitation	Opalescence	Odor/Gas Formation
DPL + EMB + Stearic acid	No	No	No	No	No	No
DPL + EMB + Capryol 90	No	No	No	No	No	No
DPL + EMB + Tween 80	No	No	No	No	No	No

4.7. Optimization of DPL-EMB NLCs

The software-generated runs were constructed (Table 9), and ANOVA was used to quantify and statistically assess the influence of independent factors on particle size, PDI, and %EE of DPL and EMB (Table 10). The findings showed that model terms were essential concerning each of the four responses and that the suggested models fit the data well.

Table 9

The response values in a Central Composite Rotatable Design (CCRD) to optimize the DPL-EMB loaded NLC, generated using Design Expert Software.

		Factor 1	Factor 2	Factor 3	Response 1	Response 2	Response 3	Response Y4
Std	Run	A: Binary mixture	B: Surfactant	C: Sonication time	Mean particle size	PDI	EE (DPL)	EE (EMB)
		%w/w	%w/v	sec	nm		%	%
1	15	1	2	40	200	0.379	86.67	85.05
2	7	3	2	40	252	0.42	93.12	91.85
3	3	1	5	40	140	0.25	86.67	85
4	2	3	5	40	132	0.32	93.46	92.12
5	8	1	2	120	111	0.269	85.45	84.9
6	18	3	2	120	218	0.356	93.1	91
7	13	1	5	120	122	0.2	86.87	84
8	14	3	5	120	181	0.24	93.13	91.5
9	6	0.318207	3.5	80	112	0.2	79.11	79.3
10	17	3.68179	3.5	80	243	0.44	93.76	93.12
11	12	2	0.977311	80	215	0.5	90.09	89.76
12	4	2	6.02269	80	119	0.19	91.39	90.02
13	11	2	3.5	12.7283	193.23	0.52	90.75	90.34
14	5	2	3.5	147.272	151	0.27	90.12	90.11
15	9	2	3.5	80	176.8	0.31	90.98	89.97
16	19	2	3.5	80	180	0.32	89.26	90.99
17	20	2	3.5	80	179	0.32	89.76	91.12
18	16	2	3.5	80	176.23	0.305	89.34	90.65
19	1	2	3.5	80	178.99	0.315	89.76	90.59
20	10	2	3.5	80	177	0.319	91.64	90.14

Table 10

Summary of arithmetical parameter for Responses Y1 (Particle size), Y2 (PDI), Y3 (%EE of DPL) and Y4 (%EE of EMB)

Response	Analysis	R ²	Adjusted R ²	Predicted R ²	SD	%CV	Model
Mean Particle size	Polynomial	0.9707	0.9572	0.8866	8.57	4.96	2F1
PDI	Polynomial	0.8091	0.7733	0.6524	0.0442	13.73	Linear
%EE of DPL	Polynomial	0.9587	0.9216	0.8078	0.9788	1.09	Quadratic
% EE of EMB	Polynomial	0.9842	0.9700	0.9066	0.6062	0.6805	Quadratic

Influence of independent variable on particle size

The degree of drug disposal in the brain and the rate at which it permeates nasal membranes are determined by particle size, a crucial quality characteristic. Ideally, the particles would be less than 200 nm [50]. The following equation was produced using the proposed 2F1 model, which had a model p-value of 0.0001, indicating the relevance of the model terms, and an F-value of 71.85, suggesting a significant model.

$$\text{MeanParticle size} = 172.86 + 31.51A - 26.91B - 11.94C - 13.50AB + 15.25AC + 19.25BC$$

The predicted R² value of 0.9572 aligns with the anticipated R² value of 0.8866, indicating a negligible deviation of under 0.2. Signal-to-noise ratio, measured with adequate precision, higher than four is preferred; the ratio of 30.052 exhibited an accurate signal. The equation indicated that the binary lipid mixture (A) had a parallel impact on particle size, whereas the surfactant (B) and sonication time (C) had a contrary impact. Particle size increased with increasing binary lipid mixture concentration (A) but decreased with increasing surfactant concentration and sonication time. The adsorption of surfactant at the interface between lipid and water led to a decrease in interfacial energy. Furthermore, sonication led to the fragmentation of bigger oil droplets. Figure 8A and Fig. 9A depict the contour plots and the correlation between the predicted and actual R².

Influence of independent variable on PDI

Poly-dispersed systems tend to form aggregates; thus, the moderately dispersed system having lower PDI is desirable to achieve a stable particulate system. PDI less than 0.5 were desired. ANOVA analysis suggested a linear model (p < 0.0001) with an F-value of 22.60, which exerted the following equation.

$$PDI = 0.3221 + 0.0470A - 0.0685B - 0.0530C$$

The level of concurrence observed between the Predicted R² value of 0.6524 and the Adjusted R² value of 0.7733 was considered acceptable, as the discrepancy between the two values was below 0.2. While the duration of sonication and surfactant concentration had a negative impact on the formulation's PDI, lipid concentration had a positive impact. The PDI increased as lipid content increased, and the PDI decreased when surfactant concentration and sonication time increased, but the significance was not as great as other responses. Figure 8B and Fig. 9B displays the contour plots and correlation between the predicted and actual R².

Influence of independent variable on entrapment efficiency of DPL and EMB

The optimum dose of a drug delivered for therapeutic effectiveness, contained in NLCs, depends on % EE, a crucial metric that significantly impacts formulation. The responses for both DPLs and EMB's percent entrapment efficiency (% EE) were suited by a quadratic model. The models proposed for these drugs were highly significant, with an F value of 25.82 for DPL and 69.36 for EMB % EE, respectively. The Predicted R² and Adjusted R² values pertaining to the % EE for DPL and EMB demonstrated a good concurrence. The impact of factors on entrapment efficiency was defined by the quadratic equations that ensued.

$$\%EEofDonepezil = 90.10 + 3.79A + 0.2912B - 0.1779C - 0.1312AB + 0.0838AC + 0.1388BC - 1.16A^2 + 0.3576B^2 + 0.2497C^2$$

$$\%EEofEmbelin = 90.59 + 3.72A + 0.0188B - 0.2202C + 0.2150AB - 0.0400AC - 0.0775BC - 1.65A^2 - 0.3458B^2 - 0.2274C^2$$

The %EE was negatively affected by the duration of sonication. Lipid content had a positive impact on it compared to surfactant. This was evident for both DPL and EMB. A drug's entrapment in a lipid depends on its solubility in the lipid. Increasing the amount of lipids results in a corresponding increase in %EE. Including surfactant diminishes the dimensions of the lipid particles, thereby increasing the number of particles available for drug entrapment and ultimately resulting in a higher %EE. However, excessive sonication can cause drug leakage from the lipid, leading to decreased %EE. According to ANOVA analysis, the model terms were highly significant (p 0.0001).

Figure 8C, D, and Fig. 9C, D displays the contour plots and correlation between the actual and predicted R².

The Design Expert software employed the numerical point system to facilitate the analysis process (Table 11) regarding Mean particle size, PDI, %EE of DPL, and %EE of EMB. The optimized NLC formulation had a Binary lipid mixture (2.21%w/v), surfactant (3.73%w/v), and sonication time (40 sec.)

Table 11

Point Prediction

Solution 1 of 15 response	Predicted Mean	Predicted Median	Observed
Mean particle size	180.73	180.73	180.2
PDI	0.374	0.374	0.373
%EE (DPL)	91.28	91.28	90.85
%EE (EMB)	91.31	91.31	89.98

5. Characterization of the optimized DPL-EMB NLCs

5.1. Surface Morphology

The NLC particles are almost globular with a black-colored center, as illustrated in Fig. 10A, according to the results of the exterior morphological investigation of the optimized DPL-EMB NLCs conducted using TEM. Solubilizing the drug within the lipids led to a blackened center within the particles. The findings of Zetasizer and the TEM analysis were well correlated.

Implying that NLC is relatively stable, optimized DPL-EMB NLC was revealed to be globe-shaped, homogenous, well-compartmentalized, and monodisperse (Fig. 10B). The Zetasizer analyzer and the particle size measured by SEM are highly correlated. Monodispersed particles showed sufficient surface charge on the nanoparticles' surfaces to keep them apart. Additionally, the negative zeta potential value supported it.

5.2. Particle Size, PDI, and zeta potential

According to publications, a particle size lesser than 200 nm is imperative to attain optimum drug permeation through a nasal membrane and neuronal uptake via several processes depending upon particle size [50], the mean diameter and PDI of the optimized combinatorial DPL and EMB loaded NLC were found to be 180.2 nm and 0.37 respectively (Fig. 11A). As per specific reports, a uniform monodisperse system is expected to exhibit a PDI close to 0.0, not surpassing 0.40. Conversely, a PDI exceeding 0.5 augurs a wide-ranging distribution of different-sized particles within the system. A moderately dispersed system with a reduced PDI is preferred to achieve a stable particulate system because poly-dispersed systems tend to form aggregates. Additionally, the moderate polydispersity of the system is established by PDI values ranging from 0.10 to 0.40 [51]. Nano lipidic carriers, such as nanoemulsions, nanoliposomes, and NLCs, are considered to have a satisfactory level of homogeneity (uniform size distribution) when their polydispersity index (PDI) is 0.40 or lower. PDI value of the optimized DPL-EMB NLCs was determined to be 0.37, signifying a stable monodisperse system.

The magnitude of the surface charge, which denotes the electrostatic motility of dispersed nanoparticles, is a common determinant of zeta potential, an evaluation of the physical stability of colloidal particles [52]. ZP is controlled by the arrangement of lipid molecules on the surface of nanoparticles, the impact of their interactions with surfactants, and the adsorption of surfactants on the interfacial surface [53]. The surface charge (Nernst potential) gradient and the extra charges produced by adsorbed ions, surfactant molecules, or stabilizer molecules in the Interfacial region are the sources of the observed zeta potential [54]. The ZP of the improved DPL-EMB NLC dispersion was 12.4. (Fig. 11B). According to the literature, zeta potential values greater than +30 or lower than -30mV are necessary for the stability of nanoparticle dispersion as well as for preventing particle aggregation [55]. ZP's negative value demonstrated the NLC globules' electrostatic repulsion to one another, inhibiting globule coalescence. Including stearic acid as a solid lipid constituent in NLCs composition may have led to a negative zeta potential. This phenomenon could be ascribed to unbound anionic fatty acid chains on the surface of the NLCs. Additionally, propylene glycol esters of the medium-chain caprylic acid (C8), which may have persisted on the outer surface of NLCs and contributed to the negative surface charge, are present in Capryol 90, which is employed as a liquid lipid in the formulation.

5.3. Entrapment efficiency and drug loading

The %EE of optimized DPL-EMB NLCs for DPL and EMB was determined as 90.85 and 89.98%, respectively. The drug loading for DPL and EMB were determined to be $9.20 \pm 0.12\%$ and $7.80 \pm 0.23\%$, respectively. The enhanced %EE and drug loading are likely ascribed to the lipid solubility of DPL and EMB and the non-crystalline molecular arrangement of NLCs.

5.4. FTIR and DSC Analysis

FT-IR spectra of lyophilized DPL-EMB NLCs (Fig. 12A) revealed that there had been no substantial alteration to the chemical structure (functional groups) of DPL and EMB when formulated into NLCs, accounting for the characteristic bands of pure DPL (conjugation Keto moiety at 1686 cm^{-1} and arenes at 1591, 1500 and 971 cm^{-1}) and pure EMB (conjugation keto moiety at 1613 cm^{-1} , C-O bond at 1193, O-H bond at 3311, C-H bond at 2861 and aromatic C-H at 2922 cm^{-1}). However, a slight shift in the wavenumber towards the right side may be due to intermolecular hydrogen bonds. The findings denote the lack of chemical susceptibility between the drugs and excipients. The DSC thermogram revealed that DPL's onset temperature (230°C) and linear melting curve justified its identity and purity. Stearic acid was found to have an onset glass transition temperature of 72.19. No change in transition was seen in the drug-loaded NLC thermogram, confirming the amorphous structure of NLC nanoparticles and the establishment of an amorphous matrix during the production of NLC nanoparticles (Fig. 12B). The molecular dissemination of the drug substances within the lipid framework results from the lack of a DPL endothermic peak in the thermogram of the DPL-EMB NLC. Stearic acid's endothermic peak (72.9 C) shifted to the left in drug-loaded NLC. The NLC comprising a blend of lipids and drug availability may be chastised for this (DPL-EMB NLCs). In NLCs, the lipid peak altitude and AUC were further decreased. Thus, after formulating the drug and lipid matrix as NLCs, a decrease in crystallinity was seen (less solid lipid crystals). This demonstrates that the oil is dispersed molecularly in the lipid mixture, causing dissonance in the lipid matrix [54]. The value of 1.78% CI indicated the low crystallinity structure of the formulated NLC.

5.5. *In Vitro* Drug Release and Release Kinetic Study

In vitro, the release of DPL and EMB from optimized NLCs and Suspension was determined by the Absorption ratio method of simultaneous estimation using UV spectrophotometry.

The optimized DPL-EMB NLC formulation and DPL-EMB Suspension were compared in an *in vitro* release experiment. The solubility of DPL and EMB in the aqueous phase is low, with log p values of 4.7 and 4.69, respectively. 1% SLS was added to the dissolving media to sustain the sink conditions. The dissolution curve obtained from DPL-EMB NLCs demonstrated a dual-phase behavior marked by an initial expeditious release preceding a sustained release. (Fig. 13). The observed lag in the release of drugs could be ascribed to the enclosed drug within a lipid structure, which facilitates sustained release via drug diffusion from the lipid matrix. Conversely, an excess amount of drug in the extraneous phase and drug adsorption onto the surface of DPL-EMB NLCs may be accountable for an initial outburst of the drugs from the formulation. The dialysis membrane junction does not impede the diffusion of DPL and EMB, and sink conditions were retained ($C_s/C_d = 45.4$ and 5.6 for DPL and EMB, respectively) for diffusion to occur from drug formulations. The optimized DPL-EMB NLCs showed initial burst release of 31.90 ± 0.27 percent for DPL and 14.87 ± 0.58 percent for EMB, whereas suspension showed 60.91 ± 1.40 percent for DPL and $47.87 \pm 1.42\%$ for EMB after 1 h. The C_s/C_d value, where C_s is the saturation solubility of the compound in the medium, and C_d is the compound's concentration in the bulk medium, should be larger than or equal to 3 to sustain sink conditions [56]. As a result, higher release was observed when DPL-EMB was suspended. Following that, optimized DPL-EMB NLCs demonstrated sustained drug release, with maximum drug release of 90.72 ± 1.00 percent for DPL and 81.30 ± 1.52 percent for EMB in 24 hours, compared to aqueous drug suspension that exhibits 97.31 ± 1.00 percent for DPL and 95.50 ± 1.52 percent for EMB in 6 hours. After 6 hours, there was a significant difference between the DPL-EMB Suspension and DPL-EMB NLC formulation when comparing the observed outcomes ($p < .05$). The Korsmeyer-Peppas model was determined to be the most convenient model for the optimized formulation, with the highest correlation coefficient values ($R^2 = 0.950$ and 0.960 for DPL and EMB, respectively). For non-Fickian diffusion-controlled release (anomalous) from non-swallowable matrix systems, the value of the release exponent "n" was determined to be in the range of 0.43 and 0.85 (0.45 and 0.58 for DPL and EMB, respectively) [57].

5.6. DPPH ASSAY

The antioxidant potential of optimized DPL-EMB NLC formulation was compared with that of ascorbic acid solution (Standard). The antioxidant efficacy of the ascorbic acid and optimized NLCs was found to be 91.10% and 89.27%, respectively. This finding confirms the antioxidant capacity of DPL-EMB NLCs. (Fig. 14)

5.7. *Ex vivo* evaluation

5.7.1. *Ex vivo* permeation studies on the nasal mucosa

Ex vivo drug permeation investigation of DPL-EMB NLCs and the suspension was accomplished using goat nares membrane. % Cumulative drug permeated in the case of DPL-EMB NLCs in 24 h was found to be 97% (DPL) and 87.29% (EMB). In contrast, in the case of DPL-EMB suspension, the % cumulative drug permeated was 64.92% (DPL) and 48.79% (EMB) in 24 h, indicating a better permeation result for optimized NLCs (Fig. 15). Steady-state flux was $92.34 \mu\text{g}/\text{cm}^2/\text{h}$ and $81.53 \mu\text{g}/\text{cm}^2/\text{h}$ for DPL and EMB in case of DPL-EMB NLCs and $77.85 \mu\text{g}/\text{cm}^2/\text{h}$, and $57.45 \mu\text{g}/\text{cm}^2/\text{h}$ for DPL and EMB in case of DPL-EMB suspension (Fig. 16). The utilization of optimized NLCs resulted in a substantial rise in drug permeation when compared to suspension.

5.7.2. *Ex-Vivo* confocal laser scanning microscopy (CLSM) visualization

Rhodamine B dye was added to the lipid matrix of OPT-DPL-EMB NLCs to see how deeply they penetrated the goat nasal mucosa. Following the treatment of methanolic NSB (6.4) of rhodamine B dye and OPT-DPL-EMB NLCs, the depth of NLC penetration was assessed by CLSM. The results of the CLSM investigation showed that, in comparison to the DPL-EMB suspension, which could only permeate the nasal mucosa up to 20 μm , OPT-DPL-EMB NLCs were highly permeable (up to 35 μm) through the multiple strata, the nasal mucosa (Fig. 17)

5.7.3. Nasal histopathological studies

In the group treated with nasal fluid, there were no indications of any inflammation or erosion. The intercellular gaps expanded in the isopropyl alcohol-treated group, indicating nasal mucosa deterioration. While nasal mucosa treated with optimized NLCs was undamaged and intact, nasal mucosa treated with drug suspension revealed minor damage (Fig. 18). DPL-EMB NLCs can be delivered by nasal route without risk.

5.8. HET-CAM Assay

The optimized DPL-EMB NLC's irritability and tolerability were evaluated through HET-CAM assay, compared to 0.9% w/v normal saline (negative control) and 0.1 N NaOH (Positive control). The test formulation (NLC) and the negative control were classified as non-irritating compared to the positive control by the mean scores. The study results indicated that normal saline had an average IS of 0.48 ± 0.01 . The positive control resulted in an average IS of 17.65 ± 0.02 , which is considered to be of severe level. The findings concur with those of Monika et al. [42]. The optimized DPL-EMB NLC and suspension-treated CAM had an average IS of 0.68 ± 0.05 and 0.73 ± 0.04 , respectively. These findings propounded the acceptability of optimized DPL-EMB NLCs for nasal administration, being nontoxic and non-irritating, as indicated in Fig. 19.

5.9. Cellular Uptake Study

After 24 hours of exposure, different-sized DPL-EMB NLCs evaluated were taken up by the cells, according to TEM images of N2a cells. (Fig. 20). TEM investigations revealed that N2a cells internalized optimized DPL-EMB NLCs primarily localized in the cytoplasm. However, the availability of NLCs in the nucleus region could not be confirmed. Results obtained concordance with a previous similar study performed by Park and associates. The study conducted by Park and colleagues revealed that the silica nanoparticles internalized by 3T3-L1 cells were confined to vacuoles, with no visible presence of nanoparticles

within the nucleus. In their subsequent micronucleus assay, they evaluated the occurrence of micronuclei in a minimum of 1000 binucleated cells for each treatment. The study found that the incidence of micronuclei in 3T3-L1 cells treated with 80 nm silica nanoparticles at 40 mg/ml was approximately 3.3%, translating to around 100 cells. TEM was utilized to examine many transected cells during their research. However, silica nanoparticles within a nuclear profile were not observed. They noted that individual 10 (11) nm silica nanoparticles were too small to be visualized in a nuclear profile through TEM [58]. Nevertheless, their findings were consistent with others using fluorescently labeled or luminescent amorphous silica nanoparticles and crystalline silica particles, which were found to be almost exclusively located in lysosomes in regions near to but not in the cell nucleus [59–61].

5.10. Stability study

The stability investigation collected and retested samples for particle size, PDI, ZP, and %EE every 30 days. None of these factors substantially varied according to the formulation. It implies that the consistency of NLC formulation was maintained for up to three months, indicating their stable character. Table 12 represents the accelerated stability data.

Table 12

Accelerated stability study for OPT-DPL-EMB NLCs

Formulation	Storage time (Months)	Temperature (° C)	RH (%)	Particle size	PDI	ZP	%EE (DPL)	%EE (EMB)
OPT-DPL-EMB NLCs	0	40 ± 2	75 ± 5	180.84 ± 0.56	0.36 ± 0.005	-12.38 ± 0.03	90.83 ± 0.01	89.77 ± 0.19
	1	40 ± 2	75 ± 5	181.47 ± 0.14	0.37 ± 0.005	-12.68 ± 0.12	90.07 ± 0.08	89.43 ± 0.08
	2	40 ± 2	75 ± 5	183.66 ± 0.18	0.38 ± 0.005	-13.28 ± 0.07	89.7 ± 0.22	88.9 ± 0.08
	3	40 ± 2	75 ± 5	184.99 ± 0.28	0.38 ± 0.005	-13.97 ± 0.13	88.98 ± 0.02	88.10 ± 0.13

6. Conclusion

The present research proposed a novel combinatorial NLC formulation for intranasal delivery for treating AD. Before the formulation development and characterization, the molecular docking studies affirmed the mechanistic approach of the pure drugs on the various target sites of target proteins associated with the pathophysiology of AD. A synergistic approach to drug combination was established via cell line studies. QBD was applied for the formulation development, and Optimization was done via CCRD. The effect of different variables on NPs preparation was investigated. The NLCs showed a 180.2 nm size, suitable for neuronal uptake and direct brain delivery. A low PDI score, 0.37, indicated that the particle size is consistent. The optimized formulation's zeta potential was at -12 mV, indicating stable and enhanced dispersion characteristics. DPL-EMB NLCs revealed sustained drug release with a maximum drug release of 90.72 ± 1.00 percent for DPL and 81.30 ± 0.52 percent for EMB in 24 h. The best-fitting model was the Korsmeyer-Peppas model with the maximum correlation coefficient (R² = 0.950 and 0.960 for DPL and EMB, respectively).

Ex vivo permeation results revealed a better permeation of optimized NLCs through goat nasal mucosa. Moreover, CLSM investigation demonstrated that OPT-DPL-EMB NLCs were highly penetrable (up to μ35 m) through the various layers of the nasal mucosa, exhibiting a higher fluorescence intensity than DPL-EMB suspension (up to 20 μm). Nasal histopathological studies revealed no signs of erosion or intercellular gaps for optimized NLCs indicating safe intranasal administration of DPL-EMB NLCs. Furthermore, the HET CAM assay showed that optimized DPL-EMB NLCs are well accepted for nasal administration, nontoxic, and non-irritating, with an irritation score of 0.68 ± 0.05. The DPL-EMB NLCs were readily engrossed by N2a cells and were majorly localized in the cytoplasm. The developed DPL and EMB-loaded NLC exhibited desirable attributes and may be used for intranasal AD therapy. The formulation needs further in vivo and clinical tests to ensure its utility in treating AD.

Declarations

Credit Author Statement

Mohd Humair Ali: Conceptualization, All investigation, Experimental work, Software, Formal analysis, Writing-original draft. **Ozair Alam:** Software. **Asad Ali:** Methodology, Experimental work. **Mohd Uzair Ali:** Writing- Review and editing. **Suhel Parvez:** Resources. **Eman Aldosari:** Funding acquisition. **Sanjula Baboota:** Data curation, review. **Javed Ali:** Project administration, Supervision, Funding acquisition.

Declaration of Interest

The authors declare that they have no known competing financial interests or personal relationships that could have appeared to influence the work reported in this paper.

Ethical Approval

The manuscript does not include any research investigations involving animals or human subjects conducted by any of the authors, exempting it from any ethical approval.

Availability of Data and Materials

Data will be made available on request.

Acknowledgments

Partially supported by the Distinguished Fellowship program (DSFP), King Saud University, Riyadh, Saudi Arabia. The authors are thankful to Prof. (Dr.) Harun M. Patel, Department of Pharmaceutical Chemistry, R.C. Patel Institute of Pharmaceutical Education, Maharashtra, for his immense support in carrying out Molecular docking investigations. The authors are also grateful to DST-FIST for facilities at Jamia Hamdard and AICTE, New Delhi, for GPAT Scholarship to the first author.

Funding

The financial support to the corresponding author from King Saud University under the Distinguished Fellowship Program is acknowledged. The authors acknowledge DST-FIST for facilities at Jamia Hamdard and AICTE, New Delhi, for GPAT Scholarship to the first author.

References

1. S. Wegmann, J. Biernat, E. Mandelkow, A current view on Tau protein phosphorylation in Alzheimer's disease, *Curr. Opin. Neurobiol.* 69 (2021) 131–138. <https://doi.org/10.1016/j.conb.2021.03.003>.
2. J. Cummings, G. Lee, A. Ritter, M. Sabbagh, K. Zhong, Alzheimer's disease drug development pipeline: 2019, *Alzheimer's Dement. Transl. Res. Clin. Interv.* 5 (2019) 272–293. <https://doi.org/10.1016/j.trci.2019.05.008>.
3. JM Ringman, A. Goate, C.L. Masters, N.J. Cairns, A. Danek, N. Graff-Radford, B. Ghetti, J.C. Morris, Genetic Heterogeneity in Alzheimer Disease and Implications for Treatment Strategies, *Curr. Neurol. Neurosci. Rep.* 14 (2014) 1–9. <https://doi.org/10.1007/S11910-014-0499-8/TABLES/1>.
4. Y. Yamazaki, N. Zhao, T.R. Caulfield, C.C. Liu, G. Bu, Apolipoprotein E, and Alzheimer disease: pathobiology and targeting strategies, *Nat. Rev. Neurol.* 2019 159. 15 (2019) 501–518. <https://doi.org/10.1038/s41582-019-0228-7>.
5. O. Pivovarov, A. Höhn, T. Grune, A.F.H. Pfeiffer, N. Rudovich, Insulin-degrading enzyme: a new therapeutic target for diabetes and Alzheimer's disease?, <https://doi.org/10.1080/07853890.2016.1197416>. 48 (2016) 614–624. <https://doi.org/10.1080/07853890.2016.1197416>.
6. D.J. Selkoe, J. Hardy, The amyloid hypothesis of Alzheimer's disease at 25 years, *EMBO Mol. Med.* 8 (2016) 595–608. <https://doi.org/10.15252/EMMM.201606210>.
7. J.L. Cummings, G. Tong, C. Ballard, Treatment Combinations for Alzheimer's Disease: Current and Future Pharmacotherapy Options, *J. Alzheimer's Dis.* 67 (2019) 779–794. <https://doi.org/10.3233/JAD-180766>.
8. S. Matsunaga, T. Kishi, N. Iwata, Memantine Monotherapy for Alzheimer's Disease: A Systematic Review and Meta-Analysis, *PLoS One.* 10 (2015). <https://doi.org/10.1371/JOURNAL.PONE.0123289>.
9. K.G. Yiannopoulou, S.G. Papageorgiou, Current and Future Treatments in Alzheimer Disease: An Update, *J. Cent. Nerv. Syst. Dis.* 12 (2020) 117957352090739. <https://doi.org/10.1177/1179573520907397>.
10. J. Rohrer, N. Lupo, A. Bernkop-Schnürch, Advanced formulations for intranasal delivery of biologics, *Int. J. Pharm.* 553 (2018) 8–20. <https://doi.org/10.1016/J.IJPHARM.2018.10.029>.
11. C.T. Lu, Y.Z. Zhao, H.L. Wong, J. Cai, L. Peng, X.Q. Tian, Current approaches to enhance CNS delivery of drugs across the brain barriers, *Int. J. Nanomedicine.* 9 (2014) 2241. <https://doi.org/10.2147/IJN.S61288>.
12. M. Yasir, U. Vir Singh Sara, I. Som, P. Gaur, M. Singh, Ameenuzzafar, Nose to Brain Drug Delivery: A Novel Approach Through Solid Lipid Nanoparticles, *Curr. Nanomedicine.* 6 (2016) 105–132. <https://doi.org/10.2174/2468187306666160603120318>.
13. R. Taliyan, V. Kakoty, K.C. Sarathlal, S.S. Kharavtekar, C.R. Karennavar, Y.K. Choudhary, G. Singhvi, Y. Riadi, S.K. Dubey, P. Kesharwani, Nanocarrier mediated drug delivery as an impeccable therapeutic approach against Alzheimer's disease, *J. Control. Release.* 343 (2022) 528–550. <https://doi.org/10.1016/J.JCONREL.2022.01.044>.
14. I. Jazuli, B. Nabi, T. Alam, S. Baboota, J.A.-J. of Pharmaceutical, undefined 2019, Optimization of nanostructured lipid carriers of lurasidone hydrochloride using Box-Behnken design for brain targeting: in vitro and in vivo studies, Elsevier. (2019). <https://doi.org/10.1016/j.xphs.2019.05.001>.
15. N. Khan, F.A. Shah, I. Rana, M.M. Ansari, F. ud Din, S.Z.H. Rizvi, W. Aman, G.Y. Lee, E.S. Lee, J.K. Kim, A. Zeb, Nanostructured lipid carriers-mediated brain delivery of Carbamazepine for improved in vivo anticonvulsant and anxiolytic activity, *Int. J. Pharm.* 577 (2020) 119033. <https://doi.org/10.1016/J.IJPHARM.2020.119033>.
16. M.I. Alam, S. Baboota, A. Ahuja, M. Ali, J. Ali, J.K. Sahni, Intranasal infusion of nanostructured lipid carriers (NLC) containing CNS acting drug and estimation in brain and blood, <http://dx.doi.org/10.3109/10717544.2013.822945>. 20 (2013) 247–251. <https://doi.org/10.3109/10717544.2013.822945>.
17. C. Zhao, J. Zhang, H. Hu, M. Qiao, D. Chen, X. Zhao, C. Yang, Design of Lactoferrin modified lipid nanocarriers for efficient brain-targeted delivery of Nimodipine, *Mater. Sci. Eng. C.* 92 (2018) 1031–1040. <https://doi.org/10.1016/J.MSEC.2018.02.004>.
18. K. Jain, S. Sood, K. Gowthamarajan, Optimization of artemether-loaded NLC for intranasal delivery using central composite design, <https://doi.org/10.3109/10717544.2014.885999>. 22 (2014) 940–954. <https://doi.org/10.3109/10717544.2014.885999>.
19. R.G. Madane, H.S. Mahajan, Curcumin-loaded nanostructured lipid carriers (NLCs) for nasal administration: design, characterization, and in vivo study, <https://doi.org/10.3109/10717544.2014.975382>. 23 (2014) 1326–1334. <https://doi.org/10.3109/10717544.2014.975382>.
20. P. Dadhania, P.R. Vuddanda, A. Jain, S. Velaga, S. Singh, Intranasal delivery of Asenapine loaded nanostructured lipid carriers: formulation, characterization, pharmacokinetic and behavioral assessment, *RSC Adv.* 6 (2016) 2032–2045. <https://doi.org/10.1039/C5RA19793G>.
21. Y. Wu, X. Song, D. Kebebe, X. Li, Z. Xue, J. Li, S. Du, J. Pi, Z. Liu, Brain targeting of Baicalin and Salvianolic acid B combination by OX26 functionalized nanostructured lipid carriers, *Int. J. Pharm.* 571 (2019) 118754. <https://doi.org/10.1016/J.IJPHARM.2019.118754>.

22. S. Hernando, E. Herran, J. Figueiro-Silva, J.L. Pedraz, M. Igartua, E. Carro, R.M. Hernandez, Intranasal administration of TAT-conjugated lipid nanocarriers loading GDNF for Parkinson's disease, *Mol. Neurobiol.* 55 (2018) 145–155. <https://doi.org/10.1007/S12035-017-0728-7>.
23. FDA, cder, HIGHLIGHTS OF PRESCRIBING INFORMATION, (n.d.). www.fda.gov/medwatch. (accessed June 22, 2023).
24. D. Spieler, C. Namendorf, T. Namendorf, M. von Cube, M. Uhr, Donepezil, a cholinesterase inhibitor used in Alzheimer's disease therapy, is actively exported out of the brain by abcb1ab p-glycoproteins in mice, *J. Psychiatr. Res.* 124 (2020) 29–33. <https://doi.org/10.1016/J.JPSYCHIRES.2020.01.012>.
25. V.K. Nuthakki, A. Sharma, A. Kumar, S.B. Bharate, Identification of embelin, a 3-undecyl-1,4-benzoquinone from *Embelia ribes* as a multitargeted anti-Alzheimer agent, *Drug Dev. Res.* 80 (2019) 655–665. <https://doi.org/10.1002/DDR.21544>.
26. S. Bhuvanendran, N.A. Hanapi, N. Ahemad, I. Othman, S.R. Yusof, M.F. Shaikh, Embelin, a potent molecule for Alzheimer's disease: A proof of concept from blood-brain barrier permeability, acetylcholinesterase inhibition, and molecular docking studies, *Front. Neurosci.* 13 (2019) 444303. <https://doi.org/10.3389/FNINS.2019.00495/BIBTEX>.
27. R. Arora, R. Deshmukh, Embelin Attenuates Intracerebroventricular Streptozotocin-Induced Behavioral, Biochemical, and Neurochemical Abnormalities in Rats, *Mol. Neurobiol.* 54 (2017) 6670–6680. <https://doi.org/10.1007/S12035-016-0182-Y/FIGURES/7>.
28. S. Manda, S. Sharma, A. Wani, P. Joshi, V. Kumar, S.K. Guru, S.S. Bharate, S. Bhushan, R.A. Vishwakarma, A. Kumar, S.B. Bharate, Discovery of a marine-derived bis-indole alkaloid fascaplysin, as a new class of potent P-glycoprotein inducer and establishment of its structure–activity relationship, *Eur. J. Med. Chem.* 107 (2016) 1–11. <https://doi.org/10.1016/J.EJMECH.2015.10.049>.
29. C.J. Morris, D. Della Corte, Using molecular docking and molecular dynamics to investigate protein-ligand interactions, <https://doi.org/10.1142/S0217984921300027>. 35 (2021). <https://doi.org/10.1142/S0217984921300027>.
30. F.J. Solis, R.J.B. Wets, Minimization by Random Search Techniques, <https://doi.org/10.1287/MOOR.6.1.19>. 6 (1981) 19–30. <https://doi.org/10.1287/MOOR.6.1.19>.
31. B. Gaba, M. Fazil, S. Khan, A. Ali, S. Baboota, J. Ali, Nanostructured lipid carrier system for topical delivery of terbinafine hydrochloride, *Bull. Fac. Pharmacy, Cairo Univ.* 53 (2015) 147–159. <https://doi.org/10.1016/J.BFOPCU.2015.10.001>.
32. S. Agarwal, Quetiapine Fumarate Loaded Nanostructured Lipid Carrier for Enhancing Oral Bioavailability: Design, Development and Pharmacokinetic Assessment, *Curr. Drug Deliv.* 18 (2021). <https://doi.org/10.2174/18755704MTA4cNTc6w>.
33. V.K. Rapalli, V. Kaul, T. Waghule, S. Gorantla, S. Sharma, A. Roy, S.K. Dubey, G. Singhvi, Curcumin loaded nanostructured lipid carriers for enhanced skin retained topical delivery: Optimization, scale-up, in-vitro characterization and assessment of ex-vivo skin deposition, *Eur. J. Pharm. Sci.* 152 (2020) 105438. <https://doi.org/10.1016/J.EJPS.2020.105438>.
34. A.C. Ortiz, O. Yañez, E. Salas-Huenuleo, J.O. Morales, Development of a nanostructured lipid carrier (NLC) by a low-energy method, comparison of release kinetics and molecular dynamics simulation, *Pharmaceutics.* 13 (2021) 531. <https://doi.org/10.3390/PHARMACEUTICS13040531/S1>.
35. I. Uddin, P. Venkata, R. Srikar, Y.P. Karunya, R. Chakraborty, R. Deepika, Synthesis and characterization of chitosan nanoparticles loaded with 6-gingerol isolated from *Zingiber officinale* Rosc, *An Int. J.* 9 (2020) 164–171. <https://doi.org/10.21276/ap.2020.9.2.14>.
36. R. Iqbal, Z. Mehmood, A. Baig, N. Khalid, Formulation and characterization of food grade O/W nanoemulsions encapsulating quercetin and Curcumin: Insights on enhancing solubility characteristics, *Food Bioprod. Process.* 123 (2020) 304–311. <https://doi.org/10.1016/J.FBP.2020.07.013>.
37. D. Deepika, H.K. Dewangan, L. Maurya, S. Singh, Intranasal Drug Delivery of Frovatriptan Succinate–Loaded Polymeric Nanoparticles for Brain Targeting, *J. Pharm. Sci.* 108 (2019) 851–859. <https://doi.org/10.1016/J.XPHS.2018.07.013>.
38. J. Weng, H.H.Y. Tong, S.F. Chow, In Vitro Release Study of the Polymeric Drug Nanoparticles: Development and Validation of a Novel Method, *Pharm.* 2020, Vol. 12, Page 732. 12 (2020) 732. <https://doi.org/10.3390/PHARMACEUTICS12080732>.
39. KY Ho, C.C. Tsai, C.P. Chen, J.S. Huang, C.C. Lin, Screening of Brazilian plant extracts for antioxidant activity by the use of DPPH free radical method, *Phyther. Res.* 15 (2001) 127–130. <https://doi.org/10.1002/PTR.687>.
40. R.K. Yadav, K. Shah, H.K. Dewangan, Intranasal drug delivery of sumatriptan succinate-loaded polymeric solid lipid nanoparticles for brain targeting, <https://doi.org/10.1080/03639045.2022.2090575>. 48 (2022) 21–28. <https://doi.org/10.1080/03639045.2022.2090575>.
41. S. Ahmad, I. Khan, J. Pandit, N.A. Emad, S. Bano, Kl. Dar, M.M.A. Rizvi, M.D. Ansari, M. Aqil, Y. Sultana, Brain targeted delivery of carmustine using chitosan coated nanoparticles via nasal route for glioblastoma treatment, *Int. J. Biol. Macromol.* 221 (2022) 435–445. <https://doi.org/10.1016/j.ijbiomac.2022.08.210>.
42. Monika, S. Sharma, M. Shrivastva, S. Kumar, S.A. Rabbani, A. Garg, Novel In-Situ NanoEmulGel (NEG) of Azithromycin with Eugenol for the Treatment of Periodontitis: Formulation Development and Characterization, *J. Clust. Sci.* 33 (2022) 2589–2600. <https://doi.org/10.1007/S10876-021-02172-8/METRICS>.
43. NW. Kang, S.Y. Yoon, S. Kim, N.Y. Yu, J.H. Park, J.Y. Lee, H.J. Cho, D.D. Kim, Subcutaneously injectable hyaluronic acid hydrogel for sustained release of donepezil with reduced initial burst release: Effect of hybridization of microstructured lipid carriers and albumin, *Pharmaceutics.* 13 (2021) 864. <https://doi.org/10.3390/PHARMACEUTICS13060864/S1>.
44. J. Choi, M.K. Choi, S. Chong, S.J. Chung, C.K. Shim, D.D. Kim, effect of fatty acids on the transdermal delivery of donepezil: In vitro and in vivo evaluation, *Int. J. Pharm.* 422 (2012) 83–90. <https://doi.org/10.1016/J.IJPHARM.2011.10.031>.
45. S.E. Desale, S. Chinnathambi, Role of dietary fatty acids in microglial polarization in Alzheimer's disease, *J. Neuroinflammation.* 17 (2020). <https://doi.org/10.1186/S12974-020-01742-3>.
46. R. Ali, S. Staufenbiel, Preparation and characterization of dexamethasone lipid nanoparticles by membrane emulsification technique, use of self-emulsifying lipids as a carrier and stabilizer, <https://doi.org/10.1080/10837450.2020.1863427>. 26 (2020) 262–268. <https://doi.org/10.1080/10837450.2020.1863427>.

47. S. Rathod, H. Desai, R. Patil, J. Sarolia, Non-ionic Surfactants as a P-Glycoprotein(P-gp) Efflux Inhibitor for Optimal Drug Delivery—A Concise Outlook, *AAPS PharmSciTech* 2022 231. 23 (2022) 1–10. <https://doi.org/10.1208/S12249-022-02211-1>.
48. S. Shaker, A. Gardouh, M. Ghorab, Factors affecting liposomes particle size prepared by ethanol injection method, *Res. Pharm. Sci.* 12 (2017) 346. <https://doi.org/10.4103/1735-5362.213979>.
49. P. Foroozandeh, S.A.M. Jusoh, S. Shamsuddin, Passive drug delivery, mechanisms of uptake, and intracellular trafficking, *Organelle Mol. Target.* (2021) 129–152. <https://doi.org/10.1201/9781003092773-5/PASSIVE-DRUG-DELIVERY-MECHANISMS-UPTAKE-INTRACELLULAR-TRAFFICKING-PARISA-FOROOZANDEH-SITI-ASMAA-MAT-JUSOH-SHAHARUM-SHAMSUDDIN>.
50. S. Cunha, B. Forbes, J.M.S. Lobo, A.C. Silva, Improving Drug Delivery for Alzheimer's Disease Through Nose-to-Brain Delivery Using Nanoemulsions, Nanostructured Lipid Carriers (NLC) and in situ Hydrogels, *Int. J. Nanomedicine.* 16 (2021) 4373. <https://doi.org/10.2147/IJN.S305851>.
51. LD. Olerile, Further Development of Near-Infrared Mediated Quantum Dots and Paclitaxel Co-loaded Nanostructured Lipid Carrier System for Cancer Theragnostic, *Technol. Cancer Res. Treat.* 19 (2020). <https://doi.org/10.1177/1533033820914308>.
52. A. Kumar, V. Kaur, A. Singh, N. Mishra, Development and characterization of paclitaxel and embelin loaded solid lipid nanoparticles for breast cancer, *J. Drug Deliv. Ther.* 10 (2020) 60–68. <https://doi.org/10.22270/JDDT.V10I1.3840>.
53. R. López-García, A. Ganem-Rondero, Solid Lipid Nanoparticles (SLN) and Nanostructured Lipid Carriers (NLC): Occlusive Effect and Penetration Enhancement Ability, *J. Cosmet. Dermatological Sci. Appl.* 05 (2015) 62–72. <https://doi.org/10.4236/JCDSA.2015.52008>.
54. A.B. Kovačević, R.H. Müller, C.M. Keck, Formulation development of lipid nanoparticles: Improved lipid screening and development of tacrolimus loaded nanostructured lipid carriers (NLC), *Int. J. Pharm.* 576 (2020) 118918. <https://doi.org/10.1016/J.IJPHARM.2019.118918>.
55. N. Manosalva, G. Tortella, M. Cristina Díez, H. Schalchli, A.B. Seabra, N. Durán, O. Rubilar, Green synthesis of silver nanoparticles: effect of synthesis reaction parameters on antimicrobial activity, *World J. Microbiol. Biotechnol.* 35 (2019) 1–9. <https://doi.org/10.1007/S11274-019-2664-3/METRICS>.
56. B. Ali, A. Khan, S. Nazir, A. Wahab, M. Ullah, M.N. Abbas, M. Mutahir, Discriminatory dissolution testing: A quality by design approach for formulation development of liquisolid compacts containing poor water soluble drug, *Lat. Am. J. Pharm.* 38 (2019) 2014–2021. https://www.researchgate.net/profile/Amjad-Khan-32/publication/339375261_Discriminatory_Dissolution_Testing_a_Quality_by_Design_Approach_for_Formulation_Development_of_Liquisolid_Compacts_/accessed June 21, 2023.
57. P.L. Ritger, N.A. Peppas, A simple equation for description of solute release I. Fickian and non-fickian release from non-swellable devices in the form of slabs, spheres, cylinders or discs, *J. Control. Release.* 5 (1987) 23–36. [https://doi.org/10.1016/0168-3659\(87\)90034-4](https://doi.org/10.1016/0168-3659(87)90034-4).
58. MVDZ Park, H.W. Verharen, E. Zwart, L.G. Hernandez, J. Van Benthem, A. Elsaesser, C. Barnes, G. McKerr, C.V. Howard, A. Salvati, I. Lynch, K.A. Dawson, W.H. De Jong, Genotoxicity evaluation of amorphous silica nanoparticles of different sizes using the micronucleus and the plasmid lacZ gene mutation assay, <https://doi.org/10.3109/17435390.2010.506016>. 5 (2011) 168–181. <https://doi.org/10.3109/17435390.2010.506016>.
59. L. Jin, R.B. Caldwell, T. Li-Masters, R.W. Caldwell, Homocysteine induces endothelial dysfunction via inhibition of arginine transport., *J. Physiol. Pharmacol.* 58 (2007) 191–206. <https://europepmc.org/article/med/17622691> (accessed June 21, 2023).
60. Y. Li, L. Sun, M. Jin, Z. Du, X. Liu, C. Guo, Y. Li, P. Huang, Z. Sun, Size-dependent cytotoxicity of amorphous silica nanoparticles in human hepatoma HepG2 cells, *Toxicol. Vitr.* 25 (2011) 1343–1352. <https://doi.org/10.1016/J.TIV.2011.05.003>.
61. K. Shapero, F. Fenaroli, I. Lynch, D.C. Cottell, A. Salvati, K.A. Dawson, Time and space resolved uptake study of silica nanoparticles by human cells, *Mol. Biosyst.* 7 (2011) 371–378. <https://doi.org/10.1039/C0MB00109K>.

Figures

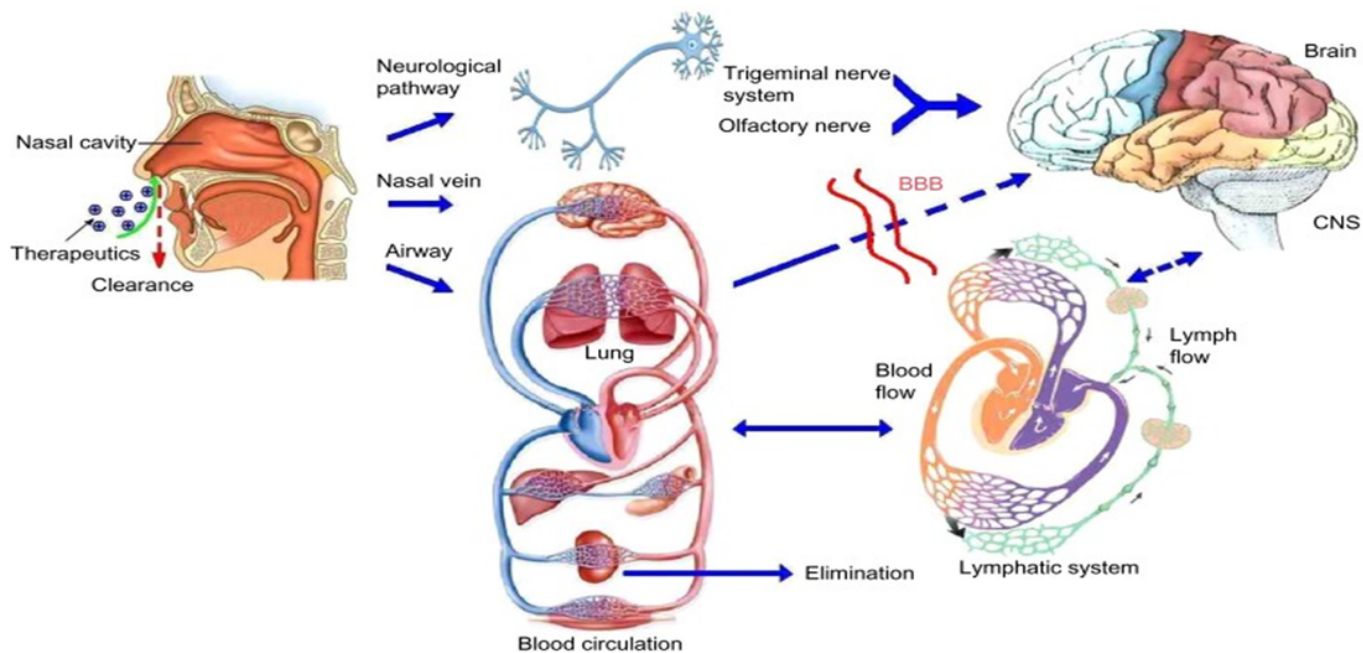


Figure 1
 Mechanism of drug transport through intranasal route (Figure reproduced from open-access Journal published by PMC under the term of creative common attribution) [11]

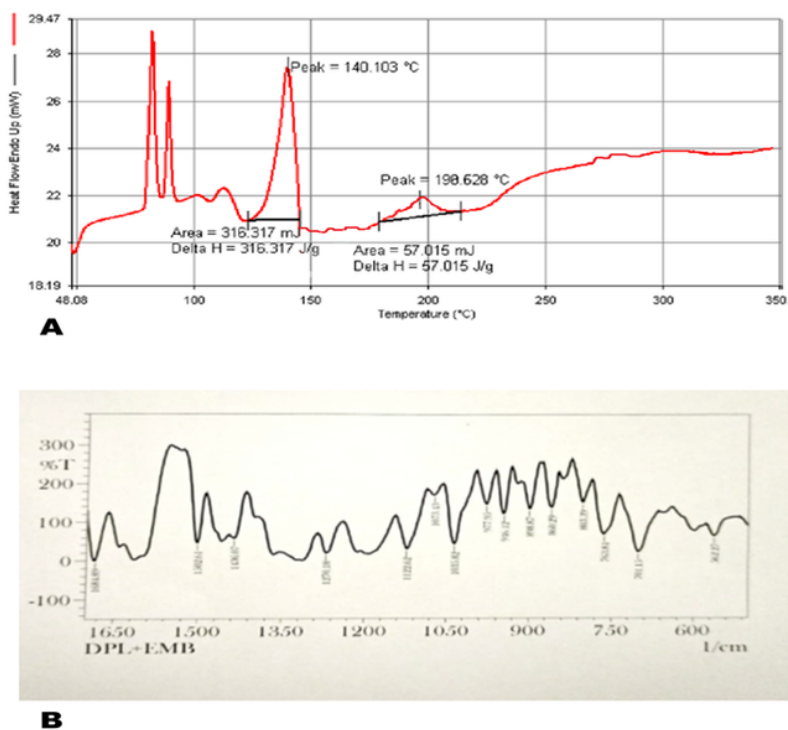


Figure 2

A) DSC thermogram of Drug mixture (DPL: EMB) kept at $40\pm 2^{\circ}\text{C}$ & $75\pm 5\%$ RH for 28 days B) FTIR spectra of Drug mixture (DPL: EMB) kept at $40\pm 2^{\circ}\text{C}$ & $75\pm 5\%$ RH for 28 days.

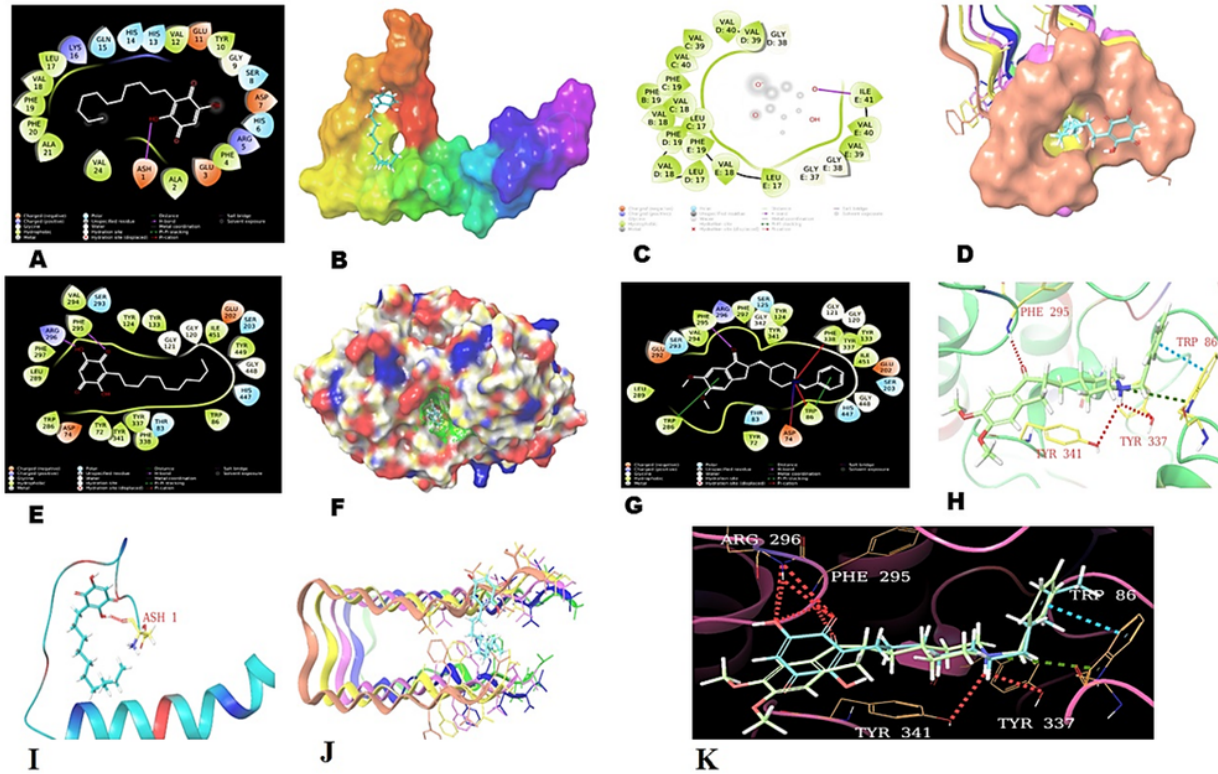


Figure 3

A) EMB interaction to 1BA4 (2D) B) Molecular surface of EMB docked to 1BA4 C) EMB interaction to 2BEG (2D) D) Receptor surface view of chains A, B, C, D, and E of EMB docked to 2BEG (3D) E) EMB interaction to 4EY7 (2D) F) Molecular surface view of EMB docked to 4EY7 (3D) G) DPL interaction to 4EY7 (2D) H) Docked pose of DPL to 4EY7 (3D) I) Docked pose of EMB to 1BA4 (3D) J) Docked pose of chains A, B, C, D and E of EMB to 2BEG (3D) K) Superimpose docked pose of DPL and EMB to 4EY7 (3D)

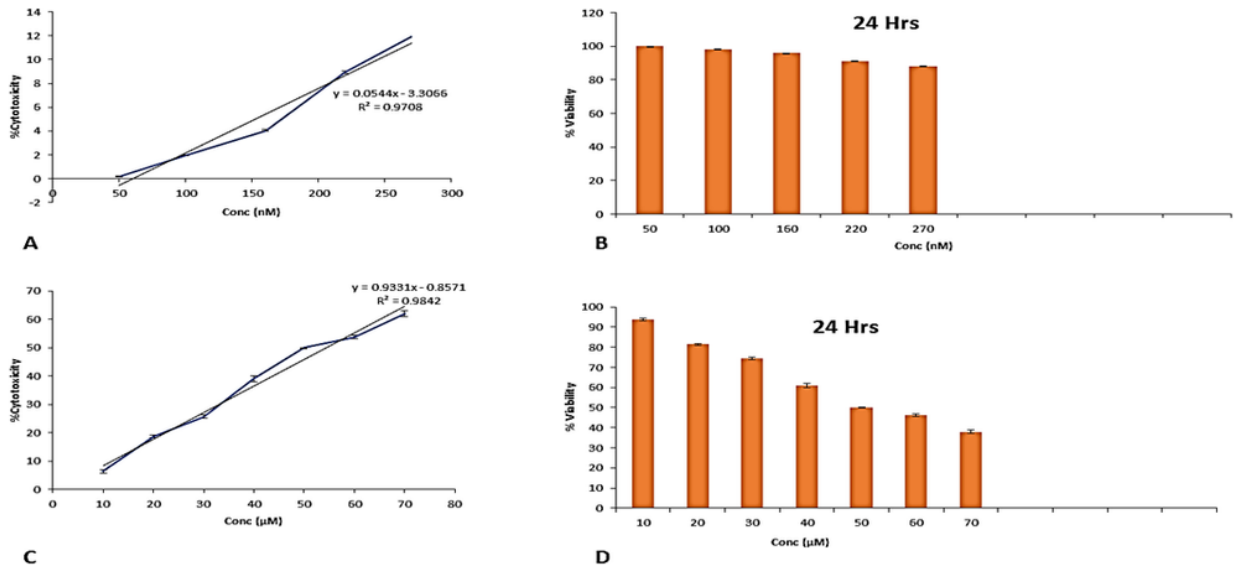


Figure 4

A) Calibration curve for % cytotoxicity for DPL B) MTT Assay of DPL C) Calibration curve for % cytotoxicity for EMB D) MTT Assay of EMB

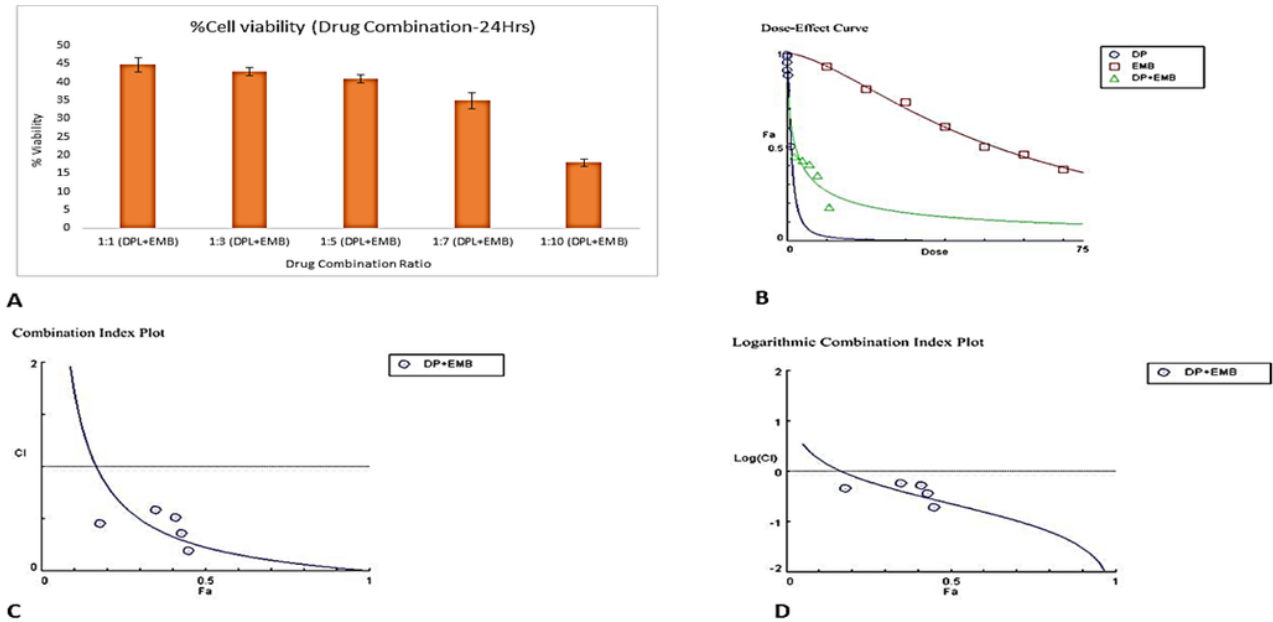


Figure 5

A) MTT Assay of Drug Combination (DPL: EMB) B) Dose effect curve C) Combination index plot D) Log Combination index plot

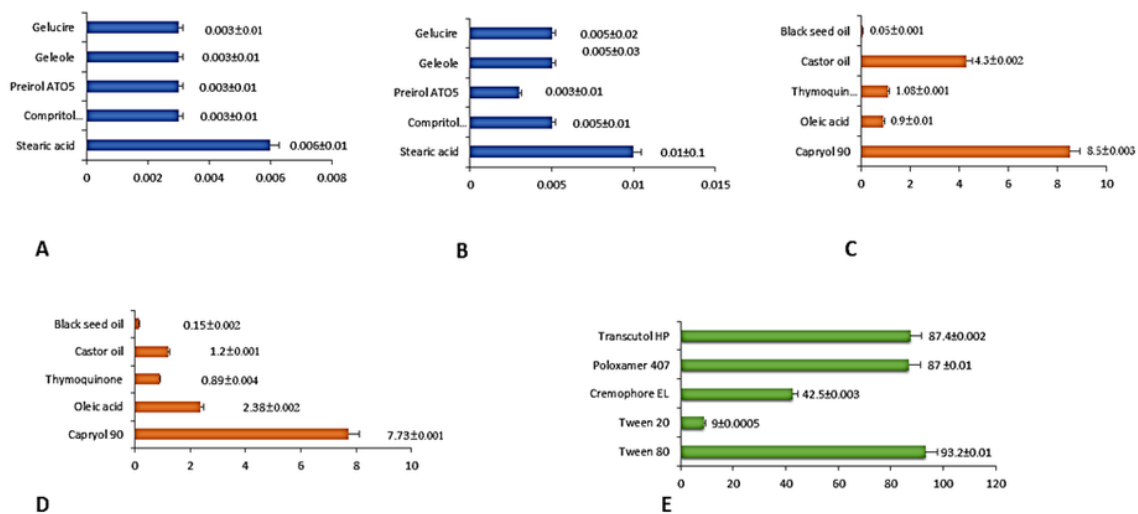


Figure 6
 A) Solubility of DPL in solid lipids B) Solubility of EMB in solid lipids C) Solubility of DPL in liquid lipids D) Solubility of EMB in liquid lipids E) % transmittance of surfactants

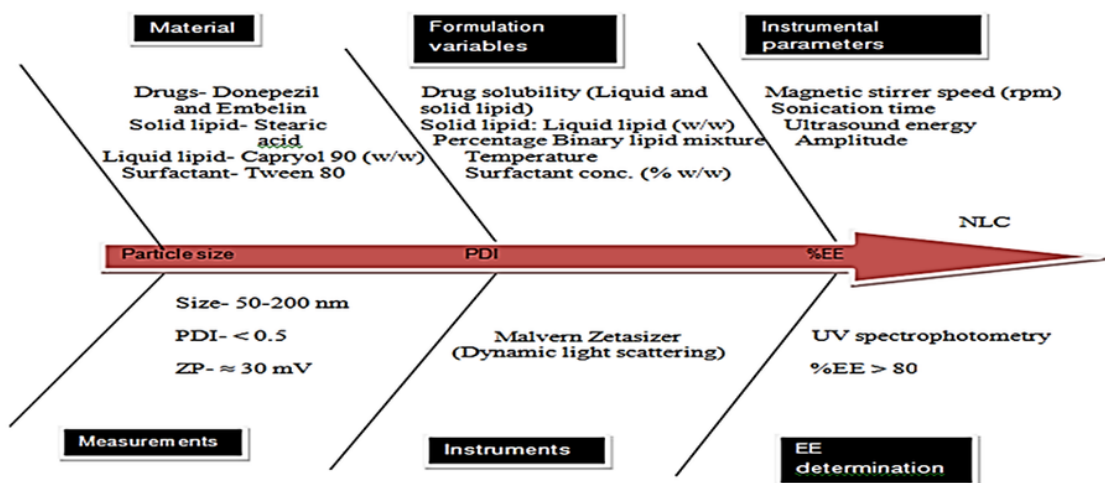


Figure 7

Ishikawa diagram showing the effects of CMAs and CPPs on CQAs of the prepared NLCs

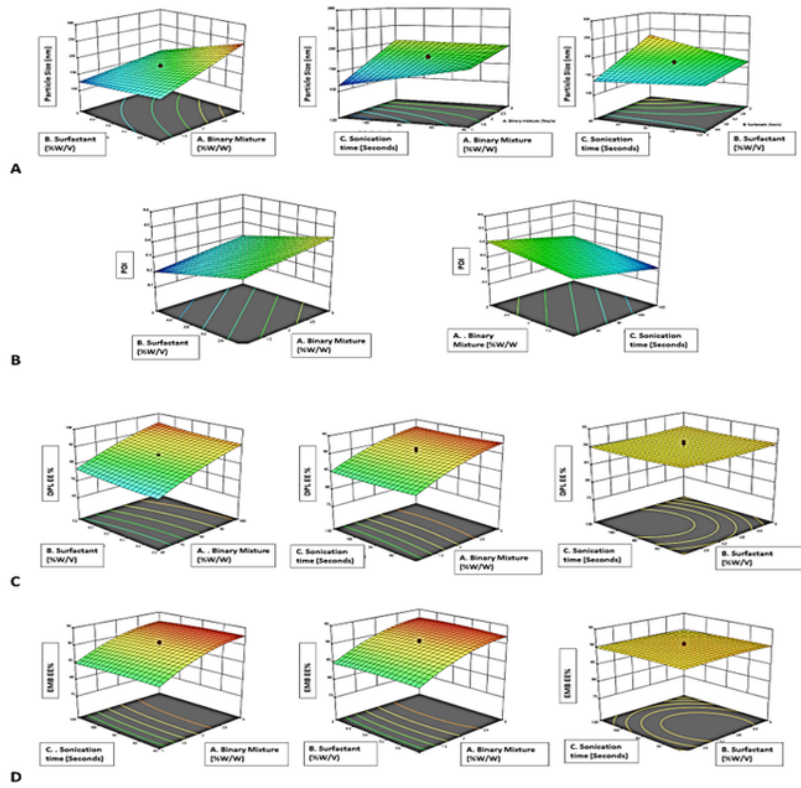


Figure 8
Contour plots depicting the effects of independent variables (Binary mixture, surfactant, and Sonication time) on A) Particle size, B) PDI, C) %EE (DPL), D) %EE (EMB)

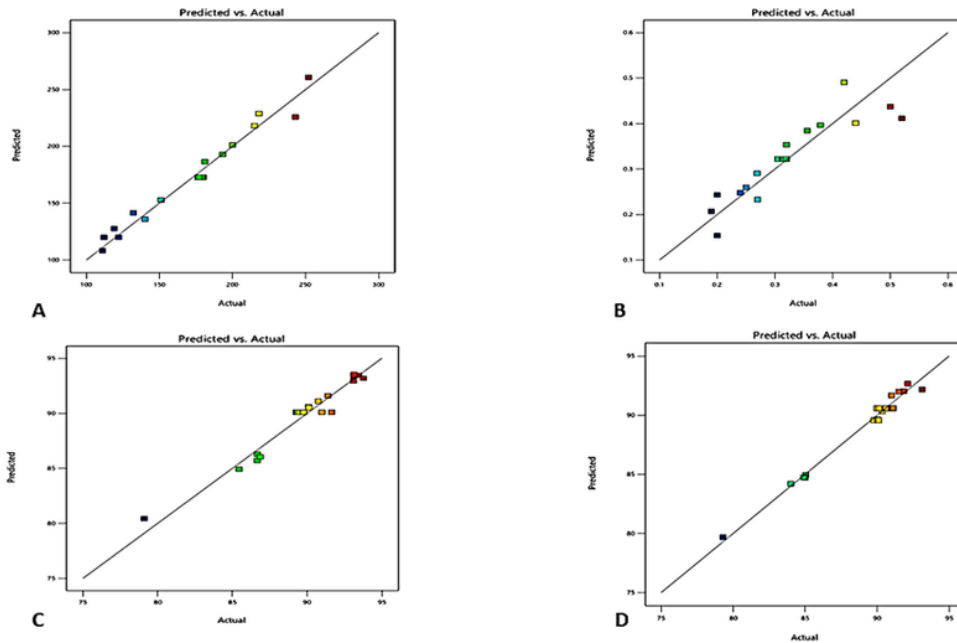
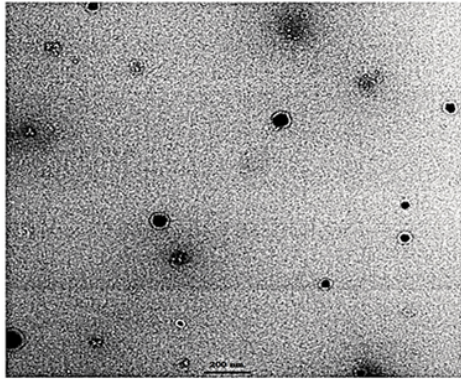
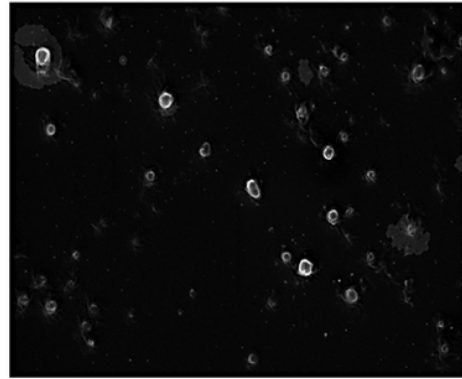


Figure 9

Correlation between the actual and predicted R-square. A) Particle size B) PDI C) %EE (DPL) D) %EE (EMB)



A



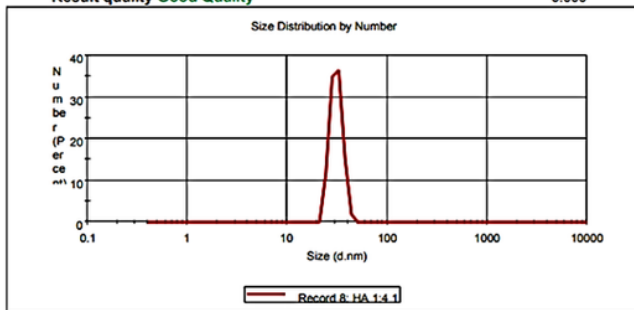
B

Figure 10

Optimized DPL-EMB NLCs A) TEM B) SEM

Results

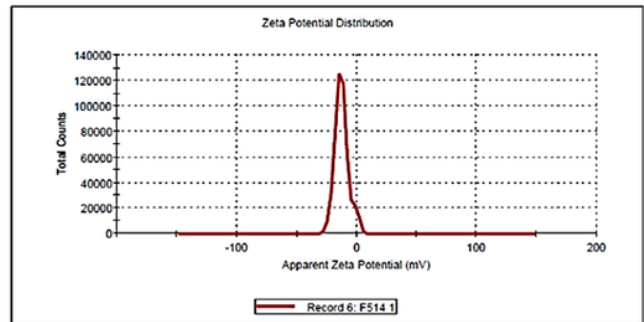
	Size (d.n...	% Number:	St Dev (d.n...
Z-Average (d.nm): 180.2	Peak 1: 52.1	100.0	4.368
Pdi: 0.373	Peak 2: 0.000	0.0	0.000
Intercept: 1.02	Peak 3: 0.000	0.0	0.000
Result quality Good Quality			0.000



A

Results

	Mean (mV)	Area (%)	St Dev (mV)
Zeta Potential (mV): -12.4	Peak 1: -12.4	100.0	5.84
Zeta Deviation (mV): 5.84	Peak 2: 0.00	0.0	0.00
Conductivity (mS/cm): 0.0825	Peak 3: 0.00	0.0	0.00
Result quality See result quality report			



B

Figure 11

A) Mean Particle size and PDI of Opt DPL-EMB NLCs B) Zeta potential of Opt DPL-EMB NLCs

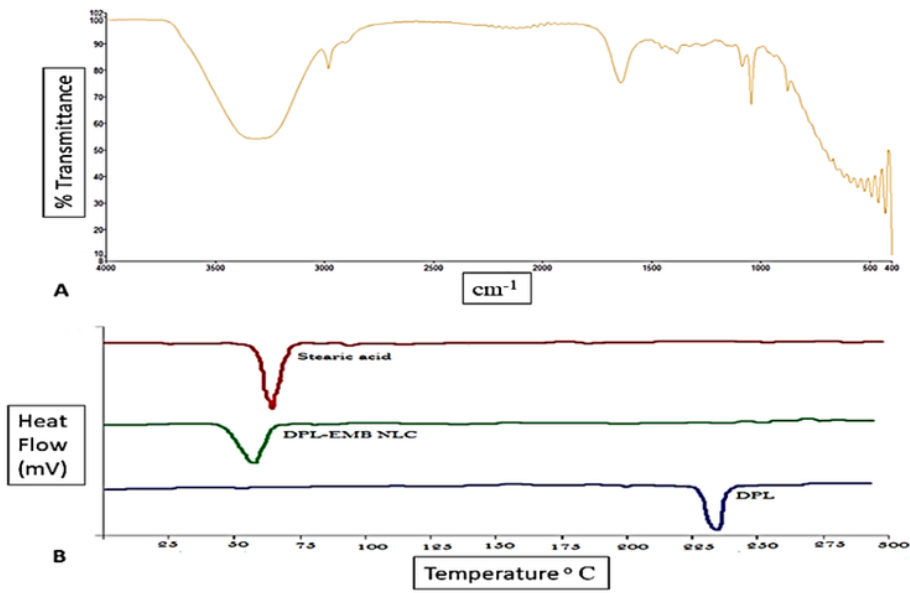


Figure 12

A) FTIR Spectra of Opt DPL-EMB NLCs B) DSC Thermogram of Stearic acid, DPL, and opt DPL-EMB NLCs

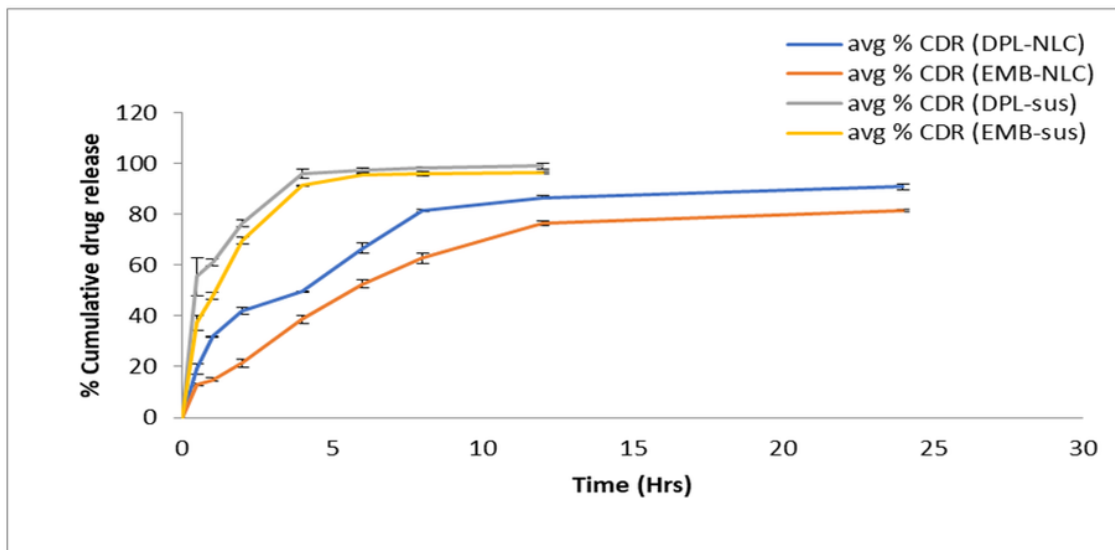


Figure 13

In vitro drug release curve for opt DPL-EMB NLCs and suspension

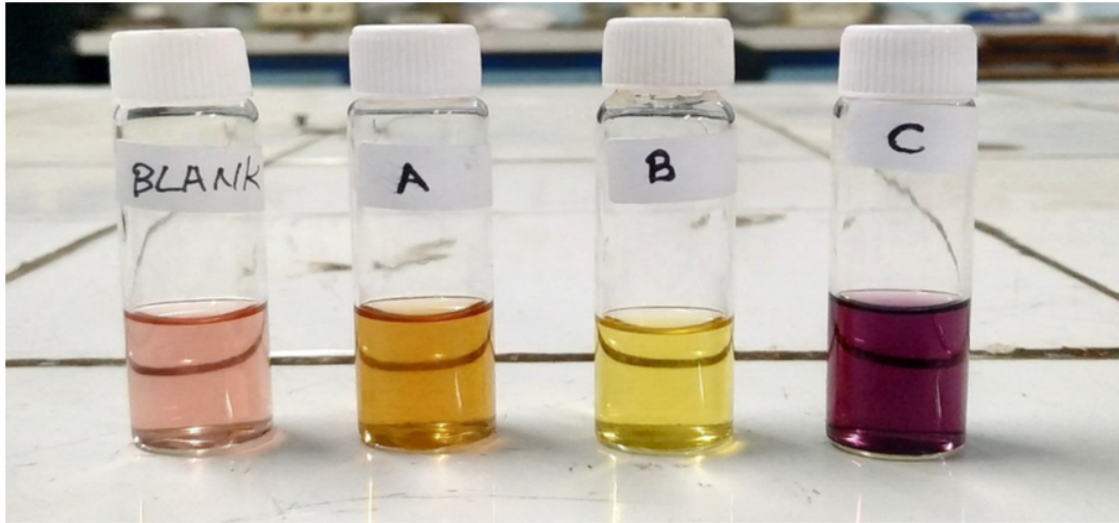


Figure 14

DPPH Assay A) Opt DPL-EMB NLCs + DPPH, B) Ascorbic acid + DPPH, C) Control (DPPH) and Blank

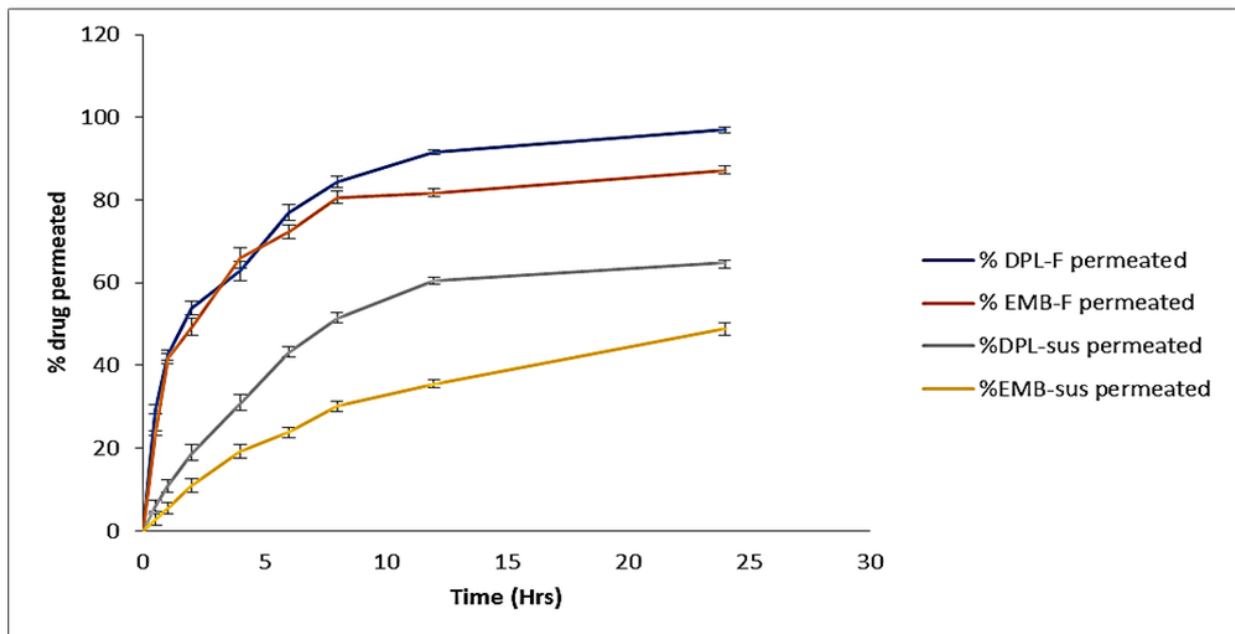


Figure 15

Ex vivo permeation of DPL and EMB from opt DPL-EMB NLCs and Suspension

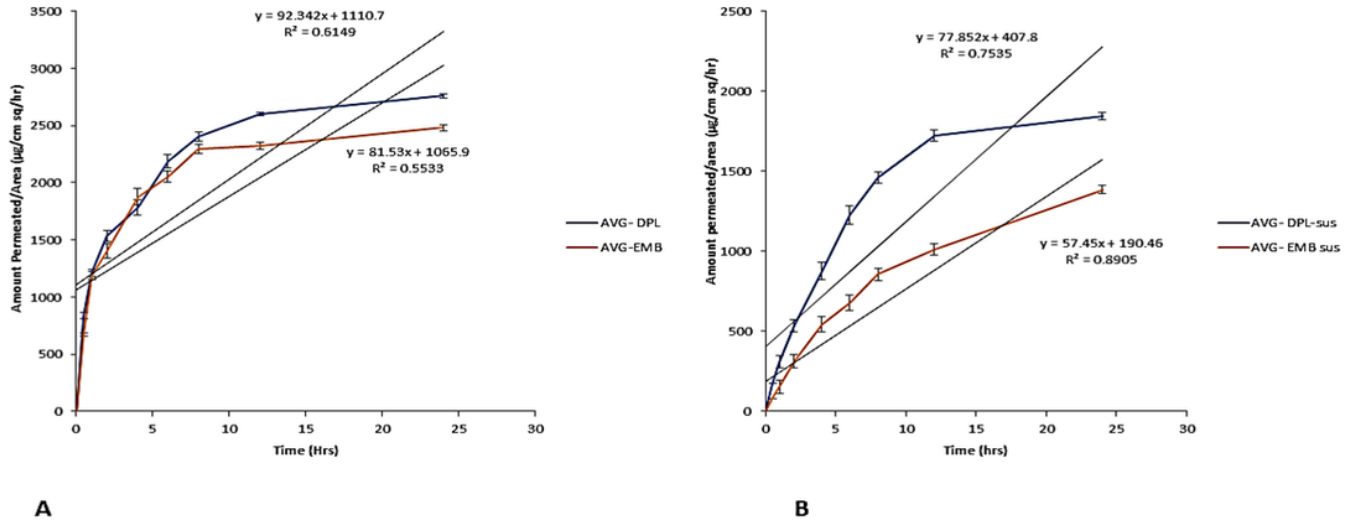


Figure 16

Flux for A) OPT DPL-EMB NLCs B) DPL-EMB suspension

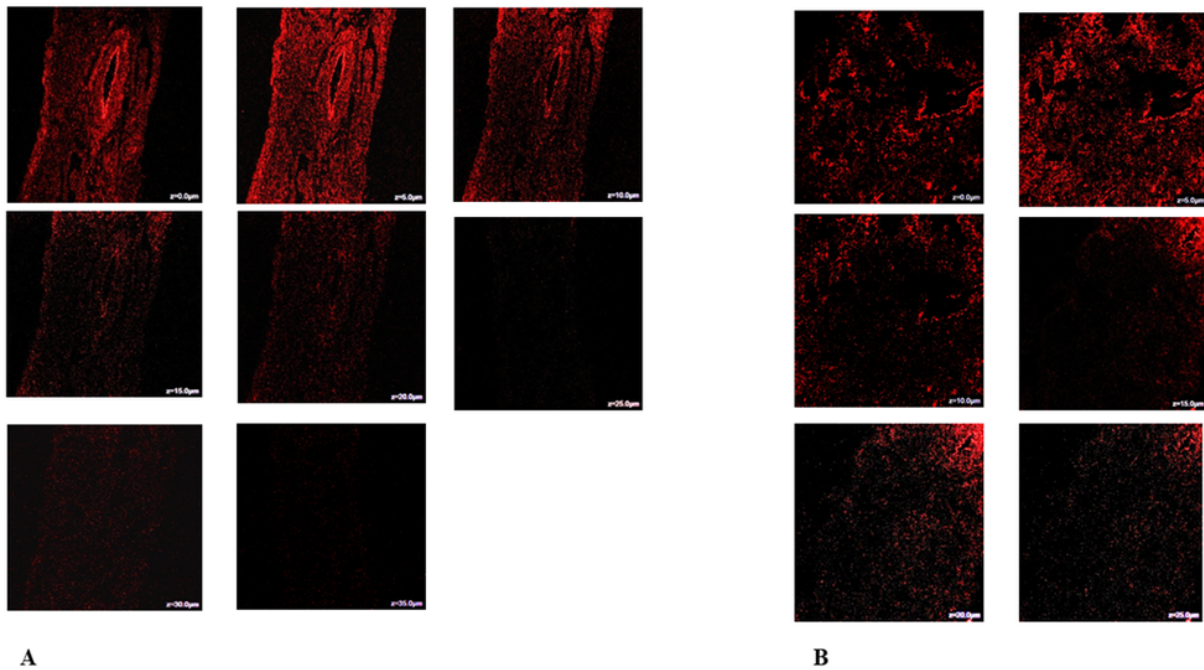


Figure 17

A) CLSM penetration for opt DPL-EMB NLCs B) CLSM penetration for DPL-EMB Suspension

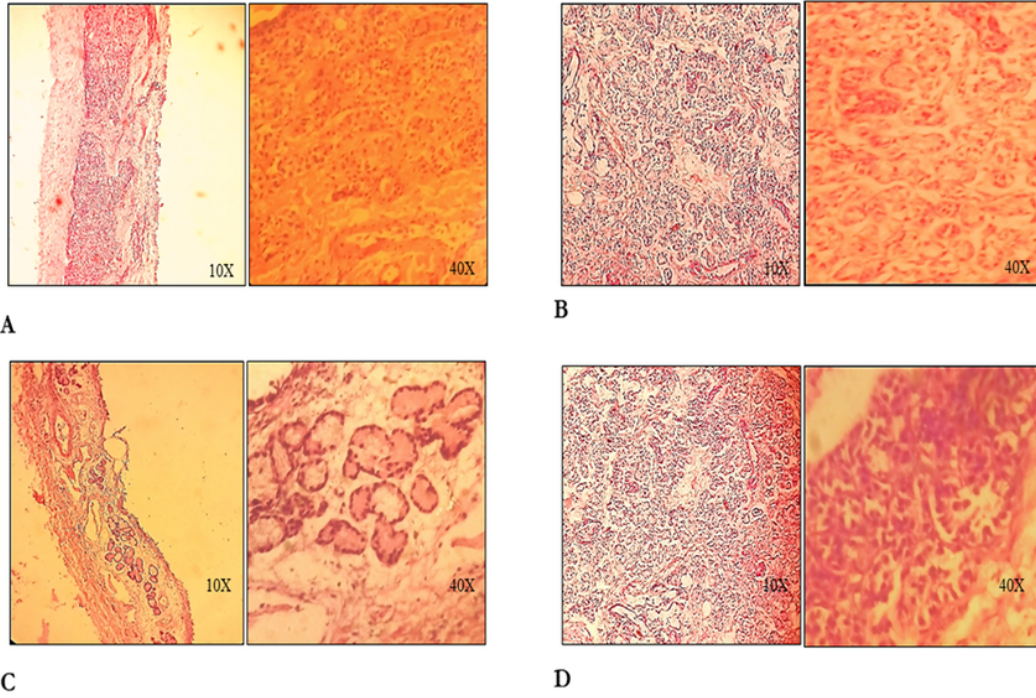


Figure 18

Histopathological slide of A) IPA treated nasal membrane B) Nasal fluid treated nasal membrane C) DPL-EMB suspension treated Nasal membrane D) Opt DPL-EMB NLC treated nasal membrane.

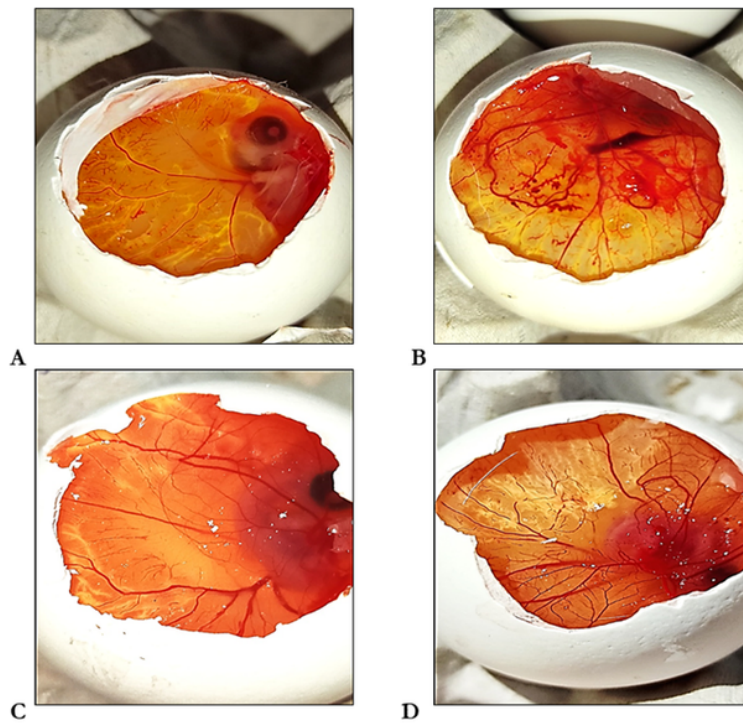


Figure 19

A) Normal saline (0.9% NaCl) treated CAM, B) 0.1N NaOH treated CAM, C) DPL-EMB NLC treated CAM, D) Suspension treated CAM.

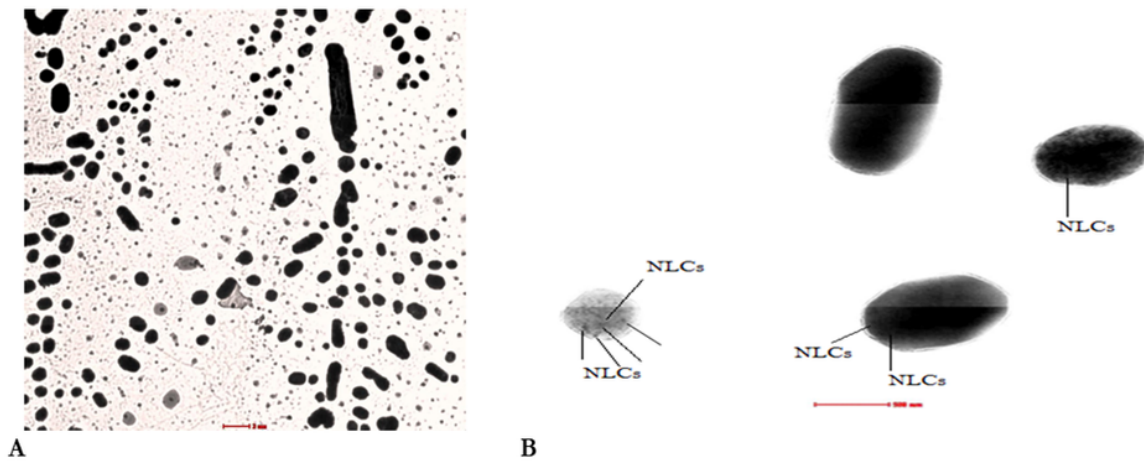


Figure 20

TEM images revealing the N2a cellular uptake of optimized DPL-EMB loaded NLCs A) N2a cells (2µm) and NLCs B) Cells demonstrating uptake of NLCs

Supplementary Files

This is a list of supplementary files associated with this preprint. Click to download.

- [GraphicalAbstract.tif](#)